Equation of state of wet granular matter

A. Fingerle* and S. Herminghaus†
Max-Planck-Institute for Dynamics and Self-Organization, Bunsenstr. 10, 37073 Göttingen, Germany
(Received 26 August 2007; published 22 January 2008)

An expression for the near-contact pair correlation function of D-dimensional weakly polydisperse hard spheres is presented, which arises from elementary free-volume arguments. Its derivative at contact agrees very well with our simulations for $D=2$. For jammed states, the expression predicts that the number of exact contacts is equal to $2D$, in agreement with established simulations. When the particles are wetted, they interact by the formation and rupture of liquid capillary bridges. Since formation and rupture events of capillary bonds are well separated in configuration space, the interaction is *hysteretic* with a characteristic energy loss E_{cb}. The pair correlation is strongly affected by this capillary interaction depending on the liquid-bond status of neighboring particles. A theory is derived for the nonequilibrium probability currents of the capillary interaction which determines the pair correlation function near contact. This finally yields an analytic expression for the equation of state, $P=P(N/V,T)$, of wet granular matter for $D=2$, valid in the complete density range from gas to jamming. Driven wet granular matter exhibits a van der Waals–like unstable branch at granular temperatures $T<T_{\mathrm{c}}$ corresponding to a first order segregation transition of clusters. For the realistic rupture length of the liquid bridge, $s_{\mathrm{crit}}=0.07d$, the critical point is located at $T_{\mathrm{c}}=0.274E_{\mathrm{cb}}$. While the critical temperature weakly depends on the rupture length, the critical density ϕ_{c} is shown to scale with s_{crit} according to $s_{\mathrm{crit}}=4d(\sqrt{\phi_{\mathrm{J}}/\phi_{\mathrm{c}}}-1)$. The segregation transition is closely related to the precipitation of granular droplets reported for the free cooling of one-dimensional wet granular matter [A. Fingerle and S. Herminghaus, Phys. Rev. Lett. **97**, 078001 (2006)], and extends the effect to higher dimensional systems. Since the limiting case of sticky bonds, $E_{\mathrm{cb}}\gg T$, is of relevance for aggregation in general, simulations have been performed which show very good agreement with the theoretically predicted coordination K of capillary bonds as a function of the bond length s_{crit}. This result implies that particles that stick at the surface, $s_{\mathrm{crit}}=0$, form isostatic clusters. An extension of the theory in which the bridge coordination number K plays the role of a self-consistent mean-field is proposed.

DOI: 10.1103/PhysRevE.77.011306 PACS number(s): 45.70.Mg, 68.08.Bc, 83.80.Fg, 45.70.Vn

I. INTRODUCTION

Dry sand trickles easily through chinks and crevices, as everyone knows well from the hour glass, or just personal experience. However, the addition of small amounts of liquid are sufficient to transform it into a plastic (or, more precisely, a viscoplastic) material. The same is true for all granular matter when a few volume percent of liquid are added, provided the latter wets the grains well and the grains are not too large. It is understood that this dramatic change, from a quasifluid to a solid behavior, is due to the formation of liquid bridges [1–10] between the granules wherever they come into contact. These liquid bridges mediate a cohesion force, and rupture as soon as the particle surfaces are separated by a distance s_{crit} which scales as the cube root of the amount of added liquid [10]. These processes of formation and rupture of liquid bridges are the main cause of the observed dramatic changes in the mechanical properties of the material. Because of the generality of the effects, it has become common to study systems with spherical grains (usually glass beads), in order to ease theoretical modeling and to avoid side effects. We decided to follow this approach.

In this work, we show analytically that the peculiar interaction by capillary bridges gives rise to a first order transition, and we compute the critical density and the critical temperature. We shall focus on the two-dimensional case, but many concepts carry over to dimensionality $D=3$. Since there is no clear observation of a first order phase transition in the hard-sphere fluid for $D\leqslant 2$ [11,12], the added liquid leads to a qualitative change. More importantly, this transition is determined entirely by the geometric and energetic properties of the capillary bridges.

A dry system of N hard spheres with diameter d confined to an area or volume V has no intrinsic energy scale, so that the equation of state is of the form $P=Tf(N/V)$ with the temperature $T=\langle mv_iv_i\rangle$ and a nonlinear density dependence, f. The defined size of hard particles is conveniently used to restate the density $n=N/V$ as the dimensionless occupied fraction $\phi=\sigma_D n d^D/(2^D D)$ (σ_D the surface of a D-dimensional unit sphere), which is the area fraction $\phi=(\pi/4)nd^2$ for two, and volume fraction $\phi=(\pi/6)nd^3$ for three dimensions.

The capillary interaction of wet granular matter has a well-defined binding energy E_{cb} [10], and it has been demonstrated experimentally [13] under realistic dynamical conditions with impact velocities typical for strongly fluidized wet granular matter that the hysteretic character of the interaction is essential: The dominant mechanism of dissipation is the hysteretic formation and rupture of capillary bridges, the energy E_{cb} of which is irreversibly taken from the kinetic energy of the granular motion whenever a liquid bridge ruptures [10]. The bridge energy has been quantified [10,13],

*axel.fingerle@ds.mpg.de
†stephan.herminghaus@ds.mpg.de

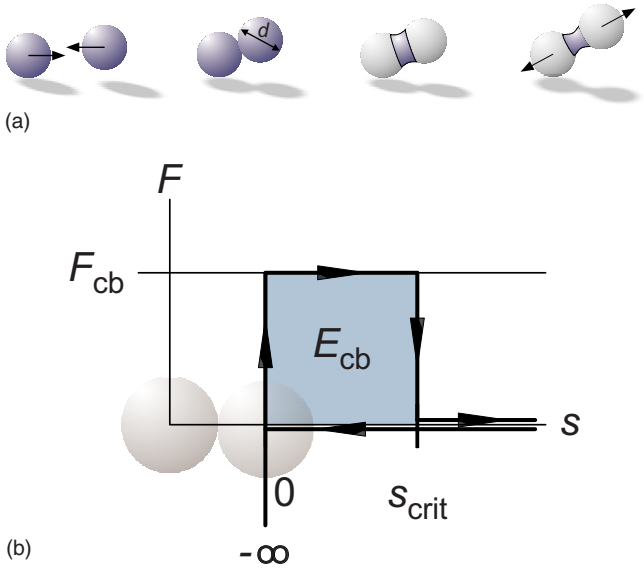

FIG. 1. (Color online) The hysteretic interaction in wet granular matter. (a) Capillary bridges form at contact and mediate an attractive force F_{cb}. At the bridge length s_{crit} the bridge becomes unstable and pinches off. (b) This hysteretic interaction by capillary bridges gives rise to a well-defined loss of energy denoted by E_{cb}. The rupture length s_{crit} is largely exaggerated for illustration. While the particle diameter d is the only length scale for dry granulates, in wet granular matter there is a second scale set by s_{crit}. A realistic value is $s_{crit} \approx 0.07d$, which is realized when 1% of the jamming volume is added by a wetting liquid (with zero contact angle). Furthermore, the bond energy E_{cb} defines an intrinsic energy scale, which is absent in dry granulates. As it is shown, the length and energy scale set by the capillary interaction give rise to a phase transition with a critical density ϕ_c and a critical granular temperature T_c.

according to which E_{cb} is proportional $d^2\sqrt{W}$. W is the volume fraction of the added liquid with respect to the total volume of the jammed granular sample. Figure 1 illustrates this hysteresis in the Minimal Capillary model [10] applied here, which assumes a constant bridge force F_{cb}. This may appear as an oversimplification at first glance, but there is increasing experimental evidence that the details of the force law are insignificant for the collective dynamics on which we focus here [10,13,14], as also confirmed from the point of view of dynamical systems theory [15,16].

Obviously, an external energy current has to be continuously injected to drive the system into a nonequilibrium steady state. In the equilibrium limit, $E_{cb} \to 0$, we will have a pressure of the form $P = Tf(\phi)$. It is the objective of this article to derive the equation of state for the hysteretic liquid bridge interaction of wet granular matter in such a driven state. In view of the intrinsic energy scale E_{cb}, this relation has to be of the form $P = P(\phi, T/E_{cb})$.

The equation of state is understood as an intrinsic property of homogeneous wet granular matter, kept in a stationary nonequilibrium state of granular temperature T. With this given temperature we may subsume various ways in which the system can be externally driven to compensate for the dissipation by rupturing liquid bridges, so that this granular temperature T is maintained over many particle diameters.

We remark that in most experimental situations involving wet granular matter, the granular temperature is a nonlinear, even discontinuous, response depending on the details of the driving, such as boundary motion or air flow in air-fluidized beds. In this article we deliberately regard the granular temperature as the *control parameter*, so that the theoretical description of the boundary coupling is conveniently separated. Yet we emphasize that for the full description of an experimental situation one has to insert the equation of state into the equation for the external energy input, and then solve for the granular temperature as the *nonlinear response* to the external driving.

We aim at describing the steady nonequilibrium states of wet granular matter, which are so multifaceted that at first glance one might think that aside from density and granular temperature further physical parameters are necessary in order to describe such a state. Yet as simulations have shown, states of wet granular matter far from equilibrium [17] are very well described by a single granular temperature T assuming a Gaussian velocity distribution, neglecting higher cumulants. Furthermore, it is known that the self-organized velocity distribution of free cooling wet granular matter has a vanishing fourth cumulant [18]. We point out that the condition of a locally isotropic and homogenous state used in this work implies that the temperature field may vary only slowly over many particle diameters so that there is no strong influence by a heat current, which would otherwise be considered as a third parameter of the local nonequilibrium state.

Throughout this study, we allow for a certain polydispersity, $0 \leqslant \Delta d/d < 0.1$. (For higher polydispersity, the dense system undergoes a kinetic glass transition [19,20]). First of all, polydispersity is frequently used in simulations and experiments to prevent the monocrystalline state. Secondly, most systems of practical relevance exhibit some polydispersity. Another characteristic of "real" granulates is that the surfaces of the grains are not ideal, bearing certain roughness. This does, however, only change the amount of liquid which must be added in order to achieve the capillary interaction: First some liquid is required to fill the crevices and tiny recesses in the grain surfaces, until the grains effectively have a smooth liquid coating, which is then completely wetted by all additional liquid. For glass beads, as those used in most of the experiments, this is typically the case above a volume fraction $W_{min} = 0.1\%$. We also require an upper limit on the volume fraction of the wetting liquid, so that the maximal length s_{crit} of liquid bridges is of the order or below the polydispersity Δd of the spheres. This is to demand that $s_{crit}/d \approx \sqrt[3]{W}/3$ is smaller than $\Delta d/d < 0.1$, so that $W < W_{max} = 2.8\%$. This happens to closely coincide with the upper limit set on the liquid content to ensure that neighboring capillary bridge do not merge [21]. For this range of the liquid content the capillary interaction is a truly pairwise interaction with the capillary force acting radially between pairs of particles. Another implication of roughness is that there is a substantial tangential friction between adjacent grains. This means that in principle one has to include all rotational degrees of freedom in the kinetic considerations for any statistical physical treatment of our system. However, we are here focussing on the effects due to the liquid capillary bridges, which mediate central forces. These do not couple to the (tangential) rotational modes. We therefore expect that the rotational degrees of freedom play, in our system, the role of a spectator heat

bath which follows the translational dynamics, but does not influence it greatly, aside from a quantitative increase of the granular specific heat. In fact, recent experiments and simulations of wet granular systems [14] show that this approach yields remarkable agreement with experimental data. In this work, we thus completely neglect all rotational degrees of freedom.

II. DRY SPHERES AS STARTING POINT

Before we add the wetting liquid to the hard sphere system, we investigate the dry case in this section and derive expressions for the pair correlation near contact, which will be extended to the wet case in the following section.

Due to their finite size, the positions of hard spheres are not distributed independently from each other, as it is the case for the point-particles of the ideal gas. The configuration space of N spheres is not V^N, but restricted to a concave subset in which the systems moves chaotically as a high dimensional billiard. With the absence of an intrinsic energy scale, the dry system is athermal, which means that a change in temperature is equivalent to rescaling the time axis. The excluded volume gives rise to correlations in the particle positions, which are measured by the pair correlation function. Denoting by $n=N/V$ the mean macroscopic particle density and by $n_{\mathrm{m}}(\mathbf{r})=\Sigma_i^N \delta(\mathbf{r}-\mathbf{r}_i)$ the microscopic density, the isotropic pair correlation $G(r)$ is defined as the probability

$$\langle n_{\mathrm{m}}(\mathbf{r})\rangle_{\text{particle at } 0} d\ \mathrm{vol} = nG(|\mathbf{r}|)d\ \mathrm{vol} = n\, g(s) d\ \mathrm{vol} \quad (1)$$

to find the center of a particle in the shell $d\ \mathrm{vol}=\sigma_D r^{(D-1)}dr$ of radius $r=r_i+r_j+s$ and thickness $dr=ds$ centered around a reference particle. We have conveniently subtracted the particle radii r_i+r_j in the last equality of Eq. (1), so that $s>0$ is the surface separation. The function $g(s)$ is advantageous for polydispersity scattered around the mean diameter d [22], because of its defined contact point, $s=0$, which is smeared out in the function $G(r)$. Furthermore it is the natural way to describe an interstitial liquid bridge between the considered pair of particles, with s the length of the bridge. For a certain liquid volume per particle and contact angle of the wetting liquid, there is a well defined critical bridge length s_{crit} at which the bridge becomes unstable and ruptures. The mean density n is factored out in Eq. (1) so that the dimensionless g would be equal to unity for all separations if there was no particle-particle correlation. Figure 2 shows the pair correlation of a fluidized state in which long range order is lost, so that $g(s)$, respectively $G(r)$, tends to unity for $r \gg d$.

The forces in wet granular matter, hard-core repulsion and liquid bridge attraction, are short-ranged and radial, acting between pairs of particles over a separation range $0<s<s_{\mathrm{crit}}$ with $s_{\mathrm{crit}} \ll d$. We are therefore interested in the short-range behavior of the pair correlation $g(s)$ up to leading order in s/d. For such short particle separations the pair correlation $g(s)$ is (up to a normalization constant) just the probability to find next neighbors at a separation s. Put in equivalent words: Decomposing the pair correlation function $g(s)=\Sigma_{k=1}^{\infty} g_k(s)$ in contributions g_k of the k's shell of Voronoï neighbors, we have $g(s)=g_1(s)$ in the range of interest, $0<s<s_{\mathrm{crit}} \ll d$. To shorten notation we suppress the subindex 1.

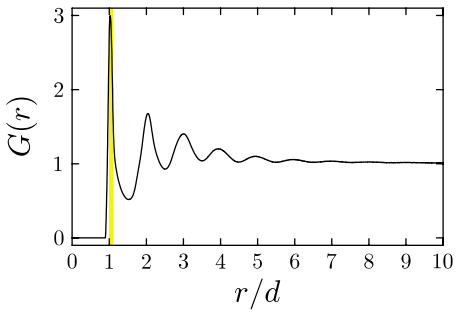

FIG. 2. (Color online) The pair correlation of wet granular matter in a fluidized state resulting from a molecular dynamics-type simulation in $D=2$ dimensions. The correlation function $G(r)$ vanishes in the range $(0,d)$ where the finite particle size leads to excluded volume. We use the function $g(s)$ with the surface separation s of neighboring particles as it is convenient for wet granular matter where interstitial liquid bridges have the length s. Note that this is not exactly identical to the function $G(d+s)$ shifted by one particle diameter d, since a realistic granular system has some polydispersity Δd around the mean diameter d. Aside from kinetic contributions, the pressure is due to the interaction forces which become dominant with increasing density. The internal forces in wet granular matter are short-ranged. Therefore our interest focuses on the sharp fall-off in the indicated range $0<s<s_{\mathrm{crit}}$ of capillary interaction. This highlighted region indicates the typical range of s_{crit}, and corresponds to the region highlighted in Fig. 4. Furthermore, we derive more detailed correlation functions, $g^{\mathrm{u}}(s)$ and $g^{\mathrm{b}}(s)$, for unbound and capillary connected pairs, respectively, in order to describe the hysteretic interaction in wet granular matter.

A. Dense limit

Figure 3 gives an overview of results by [20], [23] (Fig. 15 therein), and [24] for the phases of the two-dimensional system depending on density and polydispersity. For polydispersity below 0.1, there are two density regimes separated by the ordering transition at ϕ_{o} [25]. These transitions are a purely geometric property (i.e., excluded volume effect) of the configuration space and are therefore athermal. To compute the radial next-neighbor distribution at densities above the critical density, $\phi>\phi_{\mathrm{o}}$, we consider the Voronoï tessellation of the system, which embeds each particle into a convex polygonal cell. The sizes $\{V_i\}$ of the Voronoï cells scale as $(d+s)^D$, where the particle separation is denoted by s. For instance in $D=2$, the area of a single Voronoï cell in the ensemble is given by $\Sigma_j\{2(d+s_j)(d+s_{j+1})-[(d+s_j)^2+(d+s_{j+1})^2]\cos\alpha_j\}/(8\sin\alpha_j)$. This formula holds for direct and indirect Voronoï neighbors, and averaging over the angles α_j between neighbors yields $C(d+s)^2$ on the mean-field level, where we use a single separation s in accordance with the assumption of an isotropic state. (The assumption of isotropy will be relaxed in the discussion of clustering in wet granular matter in Sec. IV A.) In what follows we eliminate the geometry factor C in favor of the jamming density. The mean

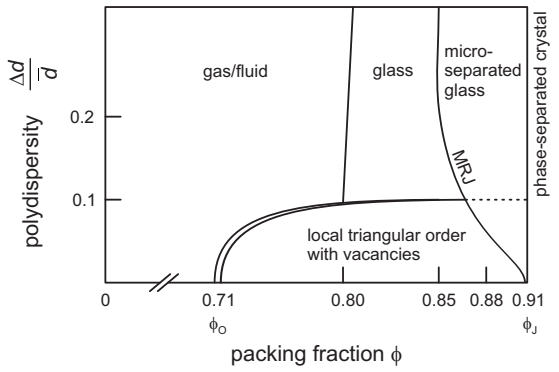

FIG. 3. This plot reviews [20,23] (Fig. 15 therein), and [24]. The athermal transitions shown are properties of the configuration space of hard disks. Since the wet granular dynamics takes place in this configuration space, results for hard disks form the starting point for a theory of wet granular matter in two dimensions. At low (gas) and moderate (fluid) densities ϕ, the configuration space is probed ergodically and the system has low shear viscosity. As density is increased, the system gets trapped in a disordered state (glass for polydispersity above 0.1), or in a state with local triangular order. Both transitions, the glass transition (vertical line at $\phi \approx 0.80$) and the ordering transition (curved line ending at $\phi_o = 0.71$) can be detected by the rapid increase of the shear viscosity η (cf. [26] for the ordering transition). While there is an athermal first order transition in three dimensions, it is at present discussed in the literature whether the transition region (double lines ending at ϕ_o) represents a fluid-solid coexistence (corresponding to a weak first order transition with a small jump of the entropy per particle) or if there is an intermediate hexatic phase (according to the Kosterlitz-Thouless-Halperin-Nelson-Young scenario) [11,12]. As the packing fraction ϕ is increased further, the islands to which the system is confined in the configuration space shrink to points. This jamming limit can be detected by the divergence of the pressure P (at fixed granular temperature) under compression (for example using the particle expansion of the Lubachevsky-Stillinger algorithm). The maximal random jammed state (MRJ, for strict jamming as defined by Torquato, Truskett, and Debenedetti [27]) is the vertical curve at the right. Densities higher than MRJ are deep in the glassy regime. From the thermodynamic point of view, the system would cluster in phases separated according to the particle size, but this eutectic freezing-transition is kinetically suppressed [23] and unreachable.

cell size $\Sigma_i^N V_i/N = V/N = 1/n$ is exactly the inverse density n. Hence

$$\left\langle \left(1 + \frac{s}{d}\right)^D \right\rangle = \frac{n(s \to 0)}{n} = \frac{\phi(s \to 0)}{\phi}, \tag{2}$$

where the triangle brackets denote averaging over next neighbors which are in contact $(s \to 0)$ with the center particle at the jamming density $\phi(s \to 0)$. We refer to those pairs of particles which come into contact at jamming as neighbors of type A, i.e., the surface separation s_A of A neighbors is

$$s_A = 0 \quad \text{at } \phi = \phi_J. \tag{3}$$

In the monodisperse limit for $D=2$, ϕ_J assumes the value of the triangular crystal, $\phi_{max} = \pi/(2\sqrt{3}) = 0.91$. Polydispersity decreases the (maximal random) jamming density ϕ_J and increases the critical density ϕ_o for the onset of triangular order as shown in Fig. 3.

1. Contribution to the contact correlation: The A neighbors

Since the Voronoï cells exchange their free volume, $V - V_{min} \propto (1 + s/d)^D - 1$, and the total volume is conserved we assume an exponential distribution of the free volume, which is well confirmed by experiments with dry granulates [28]. Conditions (2) and (3) determine the A-neighbor distribution uniquely:

$$P_A(s) d\,\mathrm{vol}(s) = \frac{D/(\sigma_D d^D)}{\phi_J/\phi - 1} \exp\left(- \frac{\left(1 + \frac{s}{d}\right)^D - 1}{\phi_J/\phi - 1} \right) d\,\mathrm{vol}(s). \tag{4}$$

The volume element for $D=2$ is

$$d\,\mathrm{vol}(s) = \sigma_D r^{(D-1)} dr = \pi d(1 + s/d) ds. \tag{5}$$

The contribution g_A which A-neighbors give to the pair correlation is equal to the A-neighbor distribution P_A (4) up to a prefactor, so that

$$g_A(s) = g_c^{at} \exp\left(- \frac{\left(1 + \frac{s}{d}\right)^D - 1}{\phi_J/\phi - 1} \right) \tag{6}$$

is determined as soon as we know the athermal contact value, $g_c^{at} = g_A(0)$. This contact value follows from the classical free volume theory [29] (which was based on [30]),

$$\frac{P}{nT} = \frac{D}{\phi_J/\phi - 1} + O(1), \tag{7}$$

in conjunction with the general relation between the particle-wall correlation g_{wall}^{at} and the pair correlation g_c^{at},

$$\frac{P}{nT} = g_{wall}^{at} = 1 + 2^{D-1} \phi g_c^{at}. \tag{8}$$

As a consequence, we obtain

$$\frac{2^{D-1}}{D} \phi g_c^{at} = \frac{1}{\phi_J/\phi - 1} \tag{9}$$

close to jamming. Expression (9) is exact for $D=1$, and has been confirmed as the asymptotic behavior of the diverging pressure close to jamming for $D=2$ [26,31] in event-driven simulation with accuracy 10^{-4}. We remark that this expression is not limited to weak polydispersity and has been confirmed for polydispersity far above 0.1 in the glass state [32,33].

Inserting Eq. (9) in Eq. (6), we have as our first central result a closed expression for the near-contact pair correlation of neighbors which form exact contacts in the jamming limit (so-called A neighbors):

$$g_A(s) = g_c^{at} \exp\left\{ - \frac{2^{D-1}}{D} \phi g_c^{at} \left[\left(1 + \frac{s}{d}\right)^D - 1 \right] \right\}. \tag{10}$$

Equation (10) implies for the derivative at contact,

$$dg_A'(0) = -2^{D-1}\phi g_A^2(0), \tag{11}$$

a quadratic dependence on the contact value $g_c^{at}=g_A(0)$. Equation (11) can be viewed as a consequence of normalization: The height of the contact peak is g_c^{at} and so the width is of the order $1/g_c^{at}$, which means that the negative slope is of the order g_c^2. In fact, writing the A-neighbor correlation function $g_A(s)$ in terms of the contact value g_c^{at}, as we did in Eq. (10), is the natural form to express the density dependence of g_A because this manifests that the coordination number of A neighbors is density independent:

$$K_A = n\int g_A d\,\mathrm{vol} = \frac{2^D D}{d}\phi g_c^{at}\int_{s=0}^{\infty}\exp\left\{-\frac{2^{D-1}}{D}\times\phi g_c^{at}\left[\left(1+\frac{s}{d}\right)^D-1\right]\right\}\left(1+\frac{s}{d}\right)^{D-1}ds$$

$$=2D. \tag{12}$$

More significantly, K_A equals exactly the isostatic contact value $2D$, which is obviously correct for particles on a line ($D=1$) and is the accepted value for ideal disks and spheres in $D=2$ and $D=3$ dimensions respectively [23,34,35]. The finding (12) is an essential confirmation of consistency of our approach, since it is independent from conventional arguments based on the rank of the rigidity matrix (which accounts for global constraints on the degrees of freedom) [34].

As the contact value g_c^{at} (9) grows to infinity in the jamming limit, $\phi\to\phi_J$, the constant integral (12) implies that $n\,g_A(s)$ becomes a delta distribution with "weight" $2D$ at contact, $s=0$.

2. Background contribution: The B neighbors

The configuration space is spanned by all particle positions $\{\mathbf{r}_i\}$. Consequently, a jammed configuration is—aside from a small fraction of rattlers [36]—an isolated configuration point, and the set of jammed configuration is a set of discrete points. When the density is slightly relaxed, a finite system remains confined to a finite environment around the jamming point (cf. [37], p. 35). As density is lowered further, these environments are no longer isolated so that the system is able to migrate between these "islands of jamming."

The stability analysis of contact networks [34,38–41] has put forth the result that frictionless spheres (except for the singular limiting case of a monodisperse crystal) jam strictly in an isostatic packing with $2D$ contacts per particle on average, as confirmed numerically [34] for $D=3$, be the state random (glass regime in Fig. 3) or locally ordered. Therefore we can identify within an island of jamming on average four neighboring particles in $D=2$ dimensions which are close to the reference particle, and which will be in contact with the reference particle, $s_A\to 0$, in the jamming limit, $\phi\to\phi_J$. These are the A neighbors with the contribution g_A to the pair correlation derived in Eq. (10). Furthermore, it is a mathematical fact that any discrete set of points in flat two-dimensional space has on average six Delaunay-Voronoï neighbors [42], two of which have no contact to the reference particle, $g_B(0)=0$. Hence, on the mean field level the following picture arises: Beside the four A neighbors there are two B neighbors which are sterically hindered by other particles from further approach to the reference particle. Summing up the contributions of A and B neighbors,

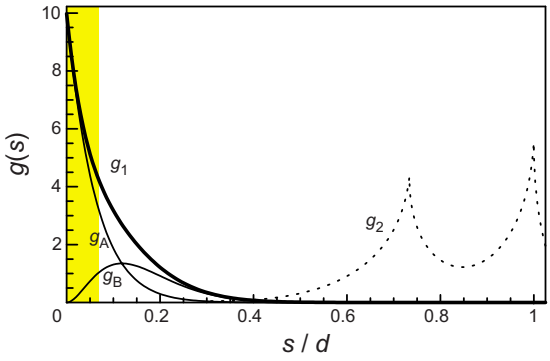

FIG. 4. (Color online) The pair correlation near contact resulting from free-volume considerations. Close to jamming we distinguish between neighbors which form exact contacts in the jamming limit [contribution g_A, Eq. (10)] and those that are blocked at positive separation s [curve g_B, Eq. (14)]. The near-contact correlation is the sum of both contributions. For this plot the density is chosen to $\phi=0.8$. The dashed curve sketches a typical second shell consisting of the second Voronoï neighbors. They are out of the interaction range, $0<s<s_{crit}$, which is indicated by the highlighted stripe.

$$g^{dense}(s) = g_A(s) + g_B(s), \tag{13}$$

gives us the pair correlation function near contact.

The pair correlation near contact which arises from these blocked states, g_B, is discussed in detail in Appendix A. The essential result is that the configuration space of blocked states tends quadratically to zero in s_B, so that to leading order the normalization of two B neighbors for $D=2$ determines the B contribution in Eq. (13):

$$g_B(s_B) = \mathcal{N}P_B(s_B) = \frac{1}{\phi c_B^3}\left(\frac{s_B}{d}\right)^2 e^{-[(1+s_B/d)^2-1]/c_B}\left[1+O\left(\frac{s_B}{d}\right)\right] \tag{14}$$

with $c_B=\phi_{max}/\phi-1$. In Fig. 4 the resulting near-contact pair correlation (13) for the dense regime is shown as the sum of g_A and g_B.

B. Dilute and moderately dense regime

In this part we turn to the free rheological regime, $0<\phi<\phi_o$. When two spheres are closer than one diameter, $s<d$, they shield each other from certain collisions events. If one was to neglect three-particle correlations, the isotropic bombardment by "third" particles gives rise to the well-known attractive depletion force first proposed by Asakura and Oosawa [43,44]. As is evident from Fig. 5, summing up equal contributions over the accessible cross section is equivalent to the pressure exerted onto the submanifold indicated by the solid line in Fig. 5(c) and denoted by Σ.

This depletion force, as well as the liquid bridge force which we will take into account in the next section, will affect the pair correlation function. A systematic way to

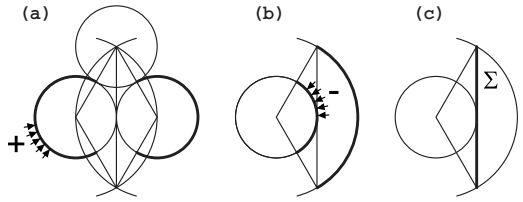

FIG. 5. Origin of the depletion force attracting neighboring particles that are separated by less than a particle diameter. One may either think of this as an entropic force, due to the decrease of excluded volume when the shells of excluded volume overlap. Equivalently one may view this as the net force due to isotropic bombardment. Obviously, the integration over the solid arc in (a) is up to a sign equivalent to the integration in (b). In (b) the integration is over the outer solid arc, which is the configuration space of the third particle's coordinate at impact. Since the integration in (b) is projected by a cos factor to give the axial symmetric force component, we can equivalently drop the cos factor and integrate over the submanifold indicated by the solid line Σ in (c).

study this effect has been worked out by Hansen *et al.* [45], resulting in a Fokker-Planck equation for the two-particle distribution function. After integrating out the momenta and the center of mass coordinates, one finds that the depletion force as well as other nonentropic pair forces (such as the liquid bridge force), give rise to a Boltzmann factor,

$$g(s) \propto \exp\left(-\frac{V(s)}{T}\right). \tag{15}$$

For the depletion force

$$F_{\mathrm{depl}} = -V'_{\mathrm{depl}} = Tng_{\mathrm{c}}^{\mathrm{at}}\Sigma, \tag{16}$$

where

$$n\, g_{\mathrm{c}}^{\mathrm{at}}\Sigma ds = \frac{dV_{\mathrm{conf}}}{V_{\mathrm{conf}}} = -d\ln g(s) \tag{17}$$

is the infinitesimal logarithmic change of the excluded area (or the configuration space per particle, V_{conf}), when the particles are separated by $s<d$, and Σ denotes the size of the corresponding section (line or area) in Fig. 5(c). At contact, $s=0$, the size of the integration section Σ is

$$\Sigma = \frac{\sigma_{D-1}}{D-1}\left(\frac{\sqrt{3}}{2}d\right)^{D-1}, \tag{18}$$

which yields V_{depl} to leading order in s. The depletion effect with the potential

$$\frac{V_{\mathrm{depl}}}{T} = \frac{9}{2}\phi g_{\mathrm{c}}^{\mathrm{at}}\frac{s}{d}\left[1-\frac{s}{3d}-\left(\frac{s}{3d}\right)^2\right] \tag{19}$$

for $D=3$ has been confirmed in [46] by computer simulations. Polydispersity is known to have a minor effect on the depletion attraction [47]. For $D=1$ Eq. (17) gives the Poisson distribution $V_{\mathrm{depl}}/T=\phi g_{\mathrm{c}}^{\mathrm{at}}s/d$ which is exact only for $D=1$.

In two dimensions, the depletion potential is

$$\frac{V_{\mathrm{depl}}}{T} = \frac{2}{\pi}\phi g_{\mathrm{c}}^{\mathrm{at}}\left(4\arctan\frac{\gamma_{\mathrm{vol}}}{W}+\gamma_{\mathrm{vol}}W-C\right) \tag{20}$$

$$= 2g_{\mathrm{c}}^{\mathrm{at}}\frac{\phi}{\phi_{\max}}\frac{s}{d}+O\left(\frac{s}{d}\right)^2 \tag{21}$$

for $D=2$ with $\gamma_{\mathrm{vol}}(s)=1+s/d$, the square root $W(s)=\sqrt{(1-s/d)(3+s/d)}$ and the constant $C=2\pi/3+\sqrt{3}$ to have $V_{\mathrm{depl}}=0$ at $s=0$. The first line (20) is valid for $0\leqslant s\leqslant d$, and the second line (21) suffices for the region of interest, $0\leqslant s\leqslant s_{\mathrm{crit}}\ll d$. For the application of results on the near-contact decay of the pair correlation function, such as Eq. (21), we prefer the exponential notation [used before in the dense case (10)] because it is most elegant to perform volume integration:

$$g_{\mathrm{AO}}^{\mathrm{dilute}}(s) = g_{\mathrm{c}}^{\mathrm{at}}\exp\left\{-\frac{\phi}{\phi_{\max}}g_{\mathrm{c}}^{\mathrm{at}}\left[\left(1+\frac{s}{d}\right)^2-1\right]\right\}\left[1+O\left(\frac{s_{\mathrm{B}}}{d}\right)^2\right] \tag{22}$$

for $D=2$. In this notation the dilute and dense behavior of the pair correlation are conveniently compared, showing that the result (22) for the gaseous-fluid regime differs by the factor $1/\phi_{\max}=1.10$ in the exponent from the dense result (10) close to jamming, so that according to Eq. (22) the depletion force falls-off slower than the configuration density $\phi g_{\mathrm{c}}^{\mathrm{at}}$. We will now show that this is due to an overestimation of the depletion force, caused by neglecting correlated three-particle events: When the plane of incidence of the third particle closely coincides with the symmetry plane Σ, the incoming particle will hit in short sequence the pair of particles considered, which increases very effectively the exchange of momentum, i.e., the depletion attraction is reduced.

To determine analytically and numerically the effect of correlated collisions which correct the Asakura-Oosawa result (22) we define the dimensionless measure

$$Z = \frac{4}{\pi}\frac{F_{\mathrm{depl}}}{nTdg_{\mathrm{c}}^{\mathrm{at}}} = -\frac{dg'_{\mathrm{c}}}{\phi g_{\mathrm{c}}^2}, \tag{23}$$

for which the Asakura-Oosawa approach (16) and (18) gives $Z_{\mathrm{AO}}=(4/\pi)\sqrt{3}\approx 2.205$ (line A in Fig. 7). When we take correlated three-particle events into account, there are three contributions. First, an attractive contribution $Z_1>0$ due to collisions on the front side of the pair, indicated by "1" in Fig. 6, which fall in the range $-\pi/2<\varphi<\pi/2$. The corresponding value Z_1 is easily integrated. Isotropy of the state demands that the angle α between the symmetry axis of the pair $P'P$ and the incoming momentum $\mathbf{p}_{\mathrm{i}}$ is uniformly distributed, as well as the impact parameter b (cf. Fig. 6). These collision parameters are related by $(\alpha,b)=(\varphi+\theta,d\sin\theta)$ to the position φ on P and the angle of incidence θ with respect to the normal of P, which implies that φ is uniformly distributed and θ is weighted by the cosine-factor $\cos\theta$. Integration over $-\pi/2<\varphi<\pi/2$ yields the axial force contribution

$$F_1 = 2Tng_{\mathrm{c}}^{\mathrm{at}}d, \tag{24}$$

so that $Z_1=8/\pi\approx 2.546$.

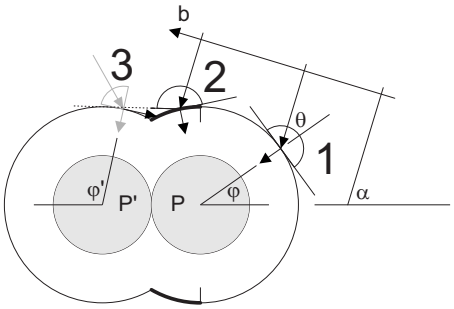

FIG. 6. Three contributions to the effective force between a pair of particles P and P'. The collisions events 1 are attractive, while the events 2 cause a weaker repulsive forces. Furthermore, the attraction is weakened by the temporally correlated collisions events 3.

Secondly, the attraction is weakened by collisions hitting P in the remaining range $\pi/2<|\varphi|<\varphi_{\max}(s)$ (which we refer to as the "broad side") giving rise to $Z_2<0$. At contact $\varphi_{\max}(s=0)$ is $2\pi/3$. For these collisions the incidence is shadowed by the partner particle P' so that the angle of incidence θ is restricted to $-\pi/2<\theta<\theta_{\max}(\varphi)$. (Confer the collision event "2" in Fig. 6.) Some trigonometry determines $\theta_{\max}(s,\varphi)$ by the relation

$$[1+\gamma_{\rm vol}(s)\cos\varphi]\sin\theta_{\max}=1-\gamma_{\rm vol}(s)\cos\theta_{\max}\sin\varphi, \tag{25}$$

which allows for an explicit function of φ at $s=0$:

$$2\cos\theta_{\max}(\varphi)=\tan\frac{\varphi}{2}-\sqrt{1+2\cos\varphi}. \tag{26}$$

After integrating over the impact momenta $p_{\rm i}$ in the rest frame of P, the axial force imposed on P is

$$F_2(s)=\frac{4}{\pi}Tng_{\rm c}^{\rm at}d\int_{\pi/2}^{\varphi_{\max}(s)}d\varphi\cos\varphi\int_{-\pi/2}^{\theta_{\max}(\varphi)}d\theta\cos^2\theta, \tag{27}$$

where the $\cos\varphi$ projects the force on the symmetry axis of the pair PP'. The $\cos\theta$ factor appears quadratically in the integrand (27) because of the cosine-distribution [or equivalent, because the Enskog collision frequency is proportional to the radial velocity $(p_{\rm i}/m)\cos\theta$], and the transferred momentum which is $p_{\rm i}\cos\theta$. Symmetry allows us to integrate over the upper half, $\pi/2<\varphi<\varphi_{\max}(s)$ in Eq. (27) and multiply by 2 with the general result

$$Z_2(s)=\frac{8}{\pi}\int_{\pi/2}^{\varphi_{\max}(s)}d\varphi\cos\varphi\left[\frac{1}{2}+\frac{\theta_{\max}(s,\varphi)}{\pi}+\frac{\sin 2\theta_{\max}(s,\varphi)}{2\pi}\right], \tag{28}$$

and the numerical value $Z_2(0)=-0.328\,13(9)$.

Thirdly, the most obvious and important correction on the three-particle level comes from double collisions denoted by 3 in Fig. 6. The third particle hits first P' (gray arrow in Fig. 6) from the broad side at $\varphi'\in(\pi/2,\theta_{\max})$. The radial component $p_i\cos\theta'$ of its incoming momentum p_i is transferred to P', which is why the third particle moves on tangentially to the circular cross section of P' with momentum $p_i\sin\theta'$ to collide shortly afterwards with particle P. Here the momentum transferred is the radial component with respect to P, $p_i\sin\theta'\cos\theta$, so that

$$F_3(s)=\frac{4}{\pi}Tng_{\rm c}^{\rm at}d\int_{\pi/2}^{\varphi_{\max}(s)}d\varphi'\cos\varphi(\varphi')\cos\theta(s,\varphi')\int_0^{\theta_{\max}(s,\varphi')}\times d\theta'\cos\theta'\sin\theta'. \tag{29}$$

The collision point on P' described by $\varphi'(\varphi)$ is related to φ (the subsequent collision point on P) by $\cos(\varphi'-\varphi)=1+\gamma_{\rm vol}(s)\cos\varphi$. The incident angle θ on P is independent of θ' and given by $\sin\theta(s,\varphi')=1+\gamma_{\rm vol}(s)\cos\varphi'$. After the elementary θ' integration we find

$$Z_3(s)=\frac{8}{\pi^2}\int_{\pi/2}^{\varphi_{\max}(s)}d\varphi'\cos\varphi(\varphi')\cos\theta(s,\varphi')\sin^2\theta_{\max}(s,\varphi'), \tag{30}$$

and $Z_3(0)=-0.091\,593(7)$. Summing up the three contributions gives $Z_{\rm corr}=\Sigma_{i=1}^3 Z_i\approx 2.127$ which is shown as the line B in Fig. 7.

Based on our numerical data shown in Fig. 7, we shall in the sequel assume the value

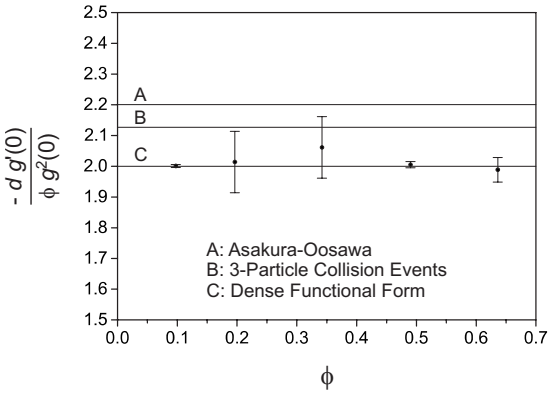

FIG. 7. Functional test of the near-contact pair correlation (32). The vertical axis is proportional to the depletion force, $F_{\rm depl}\propto -d\ln g/ds$ at contact, divided by the configuration density $\phi g_{\rm c}^{\rm at}$. This fraction Z is predicted to be density independent by Eq. (32) and to assume the value $Z=2$ (line C). Line A corresponds to the classical Asakura-Oosawa result, which is only valid for large beads immersed in a bath of small beads. In line B the corrections due to temporally correlated collisions events (derived in the text) have been taken into account. These events occur when a third particle of equal size strikes a pair of particles with a given separation $s\ll d$ as sketched in Fig. 6. We proceed using the value $Z=2$ (line C) because it agrees best with the simulation. Furthermore, $Z=2$ corresponds to a near contact correlation function which is of exactly the same form as the function $g_{\rm A}$ we use in the dense case, when expressed in terms of the configuration density $\phi g_{\rm c}^{\rm at}(\phi)$.

$$Z_{\mathrm{sim}} = 2. \tag{31}$$

By virtue of good statistics the simulation at $\phi=0.097$ gave $Z_{\mathrm{sim}}=2.0009\pm0.0050$, and Fig. 7 suggest this result to hold with few percent limits very well over the entire density regime $0<\phi<\phi_{\mathrm{o}}$ considered in this subsection. The value $Z=2$ determines the near-contact pair correlation uniquely to be

$$g^{\mathrm{dilute}}(s) = g_{\mathrm{c}}^{\mathrm{at}} \exp\left\{-\phi g_{\mathrm{c}}^{\mathrm{at}}\left[\left(1+\frac{s}{d}\right)^2-1\right]\right\}\left[1+O\left(\frac{s_{\mathrm{B}}}{d}\right)^2\right] \tag{32}$$

for $D=2$. Satisfactorily, this result (32) has exactly the same functional dependence on the configuration density $\phi g_{\mathrm{c}}^{\mathrm{at}}$ as the formula put forward for the dense case (10) in the previous subsection. While three-particle collisions are obviously important since they shift Z in the right direction, no analytic explanation for this coincidence corresponding to the value $Z=2$ is provided at present. Yet we shall see in the next section that any value other than $Z=2$ would lead to inconsistencies when we introduce the liquid bridge interaction.

We finally remark that the result (32) strongly differs from the "Poissonian fluid" [48], for which the contact correlation $g_{\mathrm{c}}^{\mathrm{at}}-1>0$ is ignored. Even at the lowest density ($\phi=0.1$) considered in Fig. 7 the Poisson fluid would give $Z_{\mathrm{Poisson}}(\phi=0.1)=1.7$ which is 15% below the simulation value, and the deviation from $Z=2$ grows with density ϕ.

III. PAIR CORRELATION UNDER THE HYSTERETIC INTERACTION

In this section we dress up the pair correlation function in order to describe the status of the liquid bonds which are created and ruptured hysteretically in wet granular matter. We will proceed in two steps. First, we introduce in Sec. III A the liquid bridges as hysteretic but forceless objects which follow the unperturbed particle dynamics. As a result, a direct relation of the dynamical system and the limiting case of isostatic granular packings [35,41] at rest is found. In Sec. III B we turn on the liquid bridge force to its physical value, so that the bridges unfold their backreaction on the granular dynamics. In the limit of low granular temperatures, $T\ll E_{\mathrm{cb}}$, the particles stick together. For this frozen state of wet granular matter the bridge coordination K is computed analytically as a function of the rupture length s_{crit}, and we find very good agreement with simulations.

A. Hysteretic coupling

Due to the hysteretic interaction, the pair correlation g is no longer a function of the particle separation s. In order to include the knowledge about the collision history the configuration space has to be enlarged in two respects: Obviously we distinguish between pairs with and without liquid bridges, which we denote by superscript indices, $g^{\mathrm{b}}(s)$ and $g^{\mathrm{u}}(s)$ respectively, for "bridged" and "unbridged" neighbors (cf. Fig. 8). In addition, time reversal-symmetry is broken by the formation of the capillary bridge at contact. Hence we distinguish approaching pairs (with a negative relative velocity) which might collide and form a liquid bridge in the future, and those that move apart so that they can rupture the liquid-bond in the future. This relative velocity is denoted by a subscript arrow.

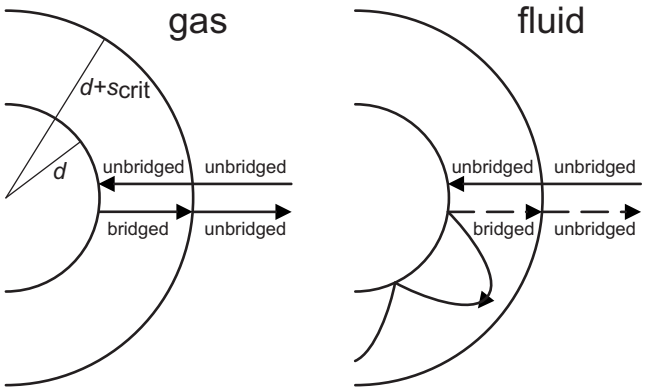

FIG. 8. The hysteretic interaction in a wet granular gas or fluid can either lead to scattering or bound states. Note that the formation and rupture of the liquid bridge is spatially separated, which gives rise to a hysteretic loss and a coupling between the pair correlation functions g^{b} for neighbors with and without, g^{u}, capillary bridge. In this sketch the maximal liquid bridge length s_{crit} is drawn largely exaggerated. For a typical volume fraction of 1% wetting liquid added to the volume of jammed granular matter one finds $s_{\mathrm{crit}}/d\approx0.07$ [10].

As we discuss the radial pair distribution, contact and rupture become the important points on the s axis of the pair correlation function. At these points the functions g^{b} and g^{u} are coupled according to the hysteretic transition of the bond status. We use an intuitive notation, writing c and r in the subscript for contact and rupture distance, respectively:

$$g^{u}_{c\leftarrow \textcircled{r}} = \begin{cases} \text{The probability for a pair} \\ \text{at rupture distance} \\ \text{approaching without} \\ \text{bridge,} \end{cases}$$

$$g^{b}_{\textcircled{c}\rightarrow r} = \begin{cases} \text{The probability for a pair} \\ \text{at contact} \\ \text{moving away with bridge,} \end{cases}$$

etc.

A configuration at contact, $s=0$ (or to be more precise: the right-sided limit $s=0+$), is denoted by a circled $\textcircled{c}$, and the rupture at $s=s_{\mathrm{crit}}$ by the circled $\textcircled{r}$. The uncircled letter allows to conveniently indicate the direction of motion with the arrow. Infinitesimally close to contact, there are four detailed correlation values: the bridge-connected and the unconnected states, either particularized by the sign of the relative velocity. The same is true for the left-sided limit $s=s_{\mathrm{crit}}-$ of the rupture point. An infinitesimal distance beyond this point, at $s=s_{\mathrm{crit}}+$, there is only the unbound state possible with the two signs for incoming and outgoing velocities. This gives us in total ten detailed pair correlation coefficients.

These are determined by the following ten equations describing the hysteretic flow of probability, as it can be read off from Fig. 8.

Conditions on the contact shell

$$g^{\mathrm{u}}_{\textcircled{c}\to r} = 0, \tag{33}$$

$$g^{\mathrm{b}}_{\textcircled{c}\to r} = g^{\mathrm{u}}_{\textcircled{c}\leftarrow r} + g^{\mathrm{b}}_{\textcircled{c}\leftarrow r}. \tag{34}$$

Equation (33) expresses that no particles rebound without a liquid-bond, but rather that all return with a bridge as stated by Eq. (34). This implies that the particle number is conserved in collisions (in contrast to the absorbent dynamics modeled in [18] for $D=1$).

Domain of capillary interaction

$$g^{\mathrm{b}}_{\textcircled{r}} = \gamma^{\mathrm{b}}(s_{\mathrm{crit}}) g^{\mathrm{b}}_{\textcircled{c}}, \tag{35}$$

$$g^{\mathrm{u}}_{\textcircled{r}} = \gamma^{\mathrm{u}}(s_{\mathrm{crit}}) g^{\mathrm{u}}_{\textcircled{c}}, \tag{36}$$

$$g^{\mathrm{u}}_{c\to\textcircled{r}} = \gamma_{\mathrm{pass}} g^{\mathrm{u}}_{c\leftarrow\textcircled{r}} \tag{37}$$

The functions $\gamma^{\mathrm{u}}(s)$ and $\gamma^{\mathrm{b}}(s)$ take into account the near-contact decay of the pair correlation without and with liquid bond, respectively. The last Eq. (37) describes spectator grains, i.e., grains which pass through the domain of possible capillary interaction without bridge formation. The fraction of these passing particles, $\gamma_{\mathrm{pass}}=1-(1+s_{\mathrm{crit}}/d)^{1-D}$ $(=1/(1+d/s_{\mathrm{crit}})$ for $D=2)$ equals the gap between the considered cross section $(2d+2s_{\mathrm{crit}})^{D-1}$ of the capillary interaction and the hard-core cross section $(2d)^{D-1}$.

Conditions on the rupture shell

$$g^{\mathrm{b}}_{c\leftarrow\textcircled{r}} = 0, \tag{38}$$

$$g^{\mathrm{u}}_{c\leftarrow\textcircled{r}} = g^{\mathrm{u}}_{c\textcircled{r}\leftarrow}, \tag{39}$$

$$g^{\mathrm{b}}_{c\to\textcircled{r}} + g^{\mathrm{u}}_{c\to\textcircled{r}} = g^{\mathrm{u}}_{c\textcircled{r}\to}. \tag{40}$$

Equations (38) and (39) state that only unbound particles enter the domain of capillary interaction, and Eq. (40) describes the rupture of a capillary bridge when the pair escapes from the domain.

The hysteretic capillary dynamics is coupled to the hard particle dynamics by the source term of new unbound pairs of particles entering the capillary interaction range.

Source term

$$g^{\mathrm{u}}_{\textcircled{c}\leftarrow r} + g^{\mathrm{u}}_{c\leftarrow\textcircled{r}}/\gamma^{\mathrm{u}}(s_{\mathrm{crit}}) = (1 - K/K_{\mathrm{sites}}) g^{\mathrm{at}}_{\textcircled{c}}. \tag{41}$$

The left-hand side is the current of approaching unbound neighbors (measured at contact). If all neighbors were unconnected, $K=0$, this current would equal the dry value $g^{\mathrm{at}}_{\textcircled{c}}$. But since there are K neighbors with bonds out of the K_{sites} "docking sites" which are sterically accessible for liquid bonds, the remaining unconnected fraction is $1-K/K_{\mathrm{sites}}$.

The final tenth equation is the stationary state condition, which demands that the rupture frequency equals the binding frequency:

Stationary state condition

$$f_{\mathrm{bind}} = f_{\mathrm{rupt}}. \tag{42}$$

These frequencies follow from the probability to have a particle on the collision or rupture shell, respectively, multiplied by the radial component of the relative velocity under the condition that the particle moves in the appropriate direction for the event to occur. This is analogous to the case $D=1$ [17], with the only difference that here we have to integrate over shells:

$$f_{\mathrm{bind}} = 2^{D+1} D \sqrt{\frac{T}{\pi}} \frac{\phi}{d} g^{\mathrm{u}}_{\textcircled{c}\leftarrow r}, \tag{43}$$

$$f_{\mathrm{rupt}} = 2^{D+1} D \sqrt{\frac{T}{\pi}} \frac{\phi}{d} g^{\mathrm{b}}_{c\to\textcircled{r}} \gamma_{\mathrm{vol}}(s_{\mathrm{crit}}). \tag{44}$$

The volume factor $\gamma_{\mathrm{vol}}(s)=(1+s/d)^{(D-1)}$ takes the increased size of the outer rupture shell as compared to the inner binding shell into account.

Eliminating those correlation coefficients that are identically zero, Eqs. (33) and (38), we can arrange the coupling equations for the domain of capillary interaction as a 6×6 matrix system:

$$\begin{array}{ll} \text{Collision:} & \\ \text{With Bridge:} & \\ \text{Unconnected:} & \\ \text{Stationarity:} & \\ \text{Spectators:} & \\ \text{Source:} & \end{array} \begin{pmatrix} 1 & 1 & -1 & 0 & 0 & 0 \\ 0 & \gamma^{\mathrm{b}} & \gamma^{\mathrm{b}} & 0 & -1 & 0 \\ \gamma^{\mathrm{u}} & 0 & 0 & -1 & 0 & -1 \\ -1 & 0 & 0 & 0 & \gamma_{\mathrm{vol}} & 0 \\ 0 & 0 & 0 & -1 & 0 & \gamma_{\mathrm{pass}} \\ 1 & 0 & 0 & 0 & 0 & 1/\gamma^{\mathrm{u}} \end{pmatrix}$$

$$\circ \begin{pmatrix} g^{\mathrm{u}}_{\textcircled{c}\leftarrow r} \\ g^{\mathrm{b}}_{\textcircled{c}\leftarrow r} \\ g^{\mathrm{b}}_{\textcircled{c}\to r} \\ g^{\mathrm{u}}_{c\to\textcircled{r}} \\ g^{\mathrm{b}}_{c\to\textcircled{r}} \\ g^{\mathrm{u}}_{c\leftarrow\textcircled{r}} \end{pmatrix} = (1 - K/K_{\mathrm{sites}}) g^{\mathrm{at}}_{\textcircled{c}} \begin{pmatrix} 0 \\ 0 \\ 0 \\ 0 \\ 0 \\ 1 \end{pmatrix}. \tag{45}$$

The γ-functions in the matrix are to be evaluated at $s=s_{\mathrm{crit}}$. As it has to be on physical grounds, this system is nonsingular with determinant $(1+s_{\mathrm{crit}}/d)^{D-1}(2+\gamma_{\mathrm{pass}})\gamma^{\mathrm{b}}(s_{\mathrm{crit}})>0$.

The last row of the system (45) describes the creation of new liquid bridges as discussed before in the context of the equivalent Eq. (41). We remark that here we used that the correlation $g^{\mathrm{at}}_{\textcircled{c}}$ of the dry system at contact has equal contributions from positive and negative relative velocities, immediately before and after the collision, which is still true for the wetted elastic particles we consider. This symmetry between positive and negative radial relative velocities is broken if one wishes to introduce a restitution coefficient $0<\epsilon<1$ to model inelastic collisions: the contact correlation of positive velocities is then increased by a factor $1/\epsilon$ as compared to the negatives.

One should see clearly the very different meaning of K

and K_{sites}. The dynamical quantity K is the *number of instantaneously existing capillary bonds*:

$$K = 2^D D\phi \frac{g_{\mathcal{C}}^{\text{b}}}{d} \int_0^{s_{\text{crit}}} \gamma^{\text{b}}(s)\gamma_{\text{vol}}(s)ds. \tag{46}$$

K rapidly decays close to zero in dilute systems. As K comes closer to the value of K_{sites} in a very dense system, the binding frequency $f_{\text{bind}} \propto g_{\mathcal{C}\leftarrow r}^{\text{u}} \propto K - K_{\text{sites}}$ (43) goes to zero because steric hindrance prohibits the formation of further capillary contacts: $K - K_{\text{sites}}$ gives the number of vacant sites for capillary bonds. Therefore K_{sites} is the maximum number of "*docking sites*" for capillary bonds. It is a pure geometric property and grows with s_{crit}, because $s_{\text{crit}} > 0$ still allows for a slight rearrangement of particles in the formation of new capillary bridges without breaking existing ones. In the limit $s_{\text{crit}} \to 0$, K_{sites} is the number of "contact sites." We therefore expect K_{sites} to equal the number of exact contacts, $2D=4$. So let us compute $K_{\text{sites}}(\phi, s_{\text{crit}})$ in the following paragraph.

The maximum number of possible bonds, K_{sites}, is an athermal function of density ϕ and the critical liquid bridge length s_{crit}. We determine K_{sites} from the obvious fact, that the granular dynamics is unaffected by the introduction of forceless bridges: for $\gamma^b = \gamma^\mu$ we recover the dry contact correlation $g_{\mathcal{C}}^b + g_{\mathcal{C}}^\mu = g_{\mathcal{C}}^{\text{at}}$. This is the athermal limit, or high temperature limit of wet granular matter.

$$\text{High temperature limit} \begin{cases} \gamma^{\text{b}} = \gamma^{\text{u}}, \\ g_{\mathcal{C}}^{\text{b}} + g_{\mathcal{C}}^{\text{u}} = g_{\mathcal{C}}^{\text{at}}. \end{cases} \tag{47}$$

From the hysteretic bridge system (45) follows in this forceless or high granular temperature limit (47)

$$\left(1 - \frac{\gamma^{\text{u}}\gamma_{\text{vol}}}{1+\gamma_{\text{pass}}}\right) K_{\text{sites}} = (1+\gamma^{\text{u}}\gamma_{\text{vol}})K, \tag{48}$$

$$g_{\mathcal{C}}^{\text{b}} = \frac{g_{\mathcal{C}}^{\text{at}}}{1+\gamma^{\text{u}}\gamma_{\text{vol}}}. \tag{49}$$

The γ functions with the argument s suppressed are understood to be evaluated at $s = s_{\text{crit}}$. Inserting Eqs. (48) and (49) in Eq. (46) yields

$$K_{\text{sites}} = 2^D D\phi g_{\mathcal{C}}^{\text{at}} \frac{\int_0^{s_{\text{crit}}} \gamma^{\text{u}}(s_{\text{crit}})\gamma_{\text{vol}}(s_{\text{crit}})ds/d}{1 - \gamma^{\text{u}}\gamma_{\text{vol}}/(1+\gamma_{\text{pass}})} \tag{50}$$

$$= 4\frac{1 - \gamma^{\text{u}} + O(s_{\text{crit}}^3)}{1 - \gamma^{\text{u}} + O(s_{\text{crit}}^2)} = 4 + O(s_{\text{crit}}). \tag{51}$$

In the last line we have set $D=2$, so that we could use Eqs. (10) and (14). The result (51) is the second important consistency test. Finding the number of exact contacts in the jamming limit to equal four in Eq. (12) showed the consistency of the free-volume argument applied there. Here in Eq. (51) we find for any density that the different function K_{sites} for the number of possible bridges sites equals four as well when $s_{\text{crit}}=0$. This is as intuitively expected and a confirmation of the consistency between the hysteretic system (45) and the near-contact pair correlation. In view of the numerical finding $Z_{\text{sim}}=2$ for the derivative at contact of the pair correlation [as defined in Eq. (23)] we remark that the entirely analytic description by the hysteretic system gives in general $K_{\text{sites}} = 8/Z + O(s_{\text{crit}})$, which is why the consistency is nontrivial and the finding $Z_{\text{sim}}=2$ fits favorably into the entire picture.

Thus the hysteretic system (45) provides a direct connection between the static granular properties captured in K_{sites} and the granular system in motion at positive granular temperature which we are treating in general. We remind that K_{sites} is determined by the steric self-hindrance and therefore a pure geometric property independent of the granular temperature. When inspecting a snapshot of a close granular packing we can find local cases of contact coordination ($s_{\text{crit}}=0$) higher than 4. These are fluctuations within the granular ensemble, while K_{sites} and K are mean-field quantities. Of course, for a finite bridge length $s_{\text{crit}} > 0$, a mean bridge coordination $K \in (0, K_{\text{sites}})$ with K_{sites} higher than four is possible due to elongated bridges, as described by Eq. (50). Before we evaluated the expression (50) of K_{sites} for positive s_{crit} (plotted in Fig. 9), it is enlightening to switch on the capillary forces in the following section because this allows us to apply K_{sites} to "frozen" wet granular matter.

B. Switching on the force of capillary bridges

Under the attraction of a liquid bridge, the pair correlation $g^{\text{b}}(s)$ of connected neighbors falls off faster than $g^{\text{u}}(s)$ for unbound particles, depending on the granular temperature T/E_{cb} compared to the bridge energy. The logarithmic derivative of the radial pair correlation is to be interpreted as the effective radial force [49,50], $\beta F = \partial_s \ln g(s)$, as discussed before in Sec. II B. This exponential dependence can be justified as the solution of the Fokker-Planck equation derived in [45]. Moreover, in the context of the hysteretic interaction of wet granular matter this exponential factor has been successfully applied in the case $D=1$ (cf. Eq. (3) in [17]). Therefore, we proceed by switching on the liquid bridge force to the physical value of the minimal capillary model [10], $F_{\text{b}} = E_{\text{cb}}/s_{\text{crit}}$, including this exponential in the short-range dependence of the pair correlation function for bridges neighbors:

$$\gamma^{\text{b}}(s,T) = \gamma^{\text{u}}(s)\exp\left(-\frac{E_{\text{cb}}}{T}\frac{s}{s_{\text{crit}}}\right). \tag{52}$$

At low granular temperatures this exponential gives rise to shorter average bridge lengths, and describes the reduced probability that a bridge reaches its critical length s_{crit}. Therefore the hysteretic system (45) describes the sticking of particles and the onset of clustering.

We have discussed in Sec. III A that steric effects in the dynamical system limit the mean number of bonds to a maximum of K_{sites}, and we derived that K_{sites} converges to the number of isostatic contacts in the limit $s_{\text{crit}} \to 0$. Here this connection is put on firm grounds with a clear physical interpretation attributed to K_{sites}: K_{sites} *is the bridge coordination K of solid wet granular matter.*

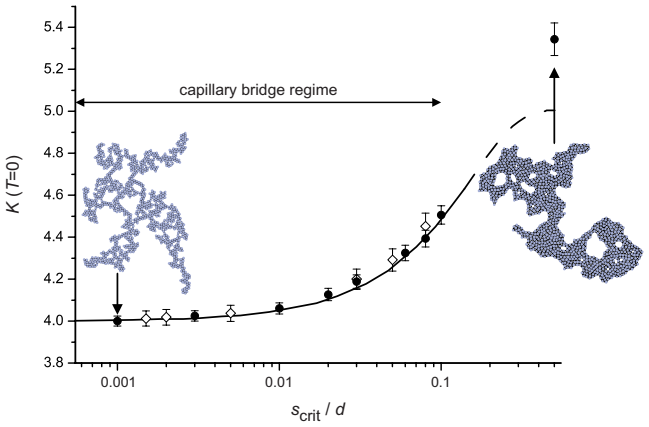

FIG. 9. (Color online) The capillary bridge coordination K in the low temperature limit, $T \ll E_{cb}$. As proven in the text, K converges to the athermal function $K_{sites}(\phi, s_{crit})$ in this low temperature limit. The solid line is $K_{sites}(\phi_o, s_{crit})$ over a wide range of maximal bridge lengths s_{crit}. Points represent final states of free cooling simulations with 1000 particles of uniformly distributed polydispersity $\Delta d = 0.06d$. The open symbols are clusters with winding number one (cylindrical topology), connected over one periodic boundary on a rectangular domain. Such structures have internal tensile strength which necessitates a slightly increased coordination, visible as a small shift compared to the closed symbols which represent localized clusters (as the two examples drawn in the plot). As predicted by Eq. (51) of the presented theory, the structures emerging with exact contacts, $s_{crit} \to 0$, are found to be precisely isostatic, $K_{sites} = 4$. The line is the analytic result (50), for which very good agreement is found with the simulations over the entire range of the capillary bridge regime, $0 < s < 0.2r$ (with r the particle radius), which is indicated in the figure. Beyond this regime, the theory does not hold because in the derivation we limited ourselves to the leading order in s_{crit}/d. More importantly, the rupture length s_{crit} cannot be further increased beyond the capillary regime by simply increasing the liquid content in the granular sample. As mentioned in the introduction, liquid bridges residing on the same sphere would rather merge [21] into more complicated objects.

Proof of $K \to K_{sites}$ in the low temperature limit. Solving Eq. (45) for K/K_{sites}, we obtain

$$\frac{K(T, s_{crit}, \phi)}{K_{sites}(s_{crit}, \phi)} = \frac{1}{1 + X(T)/Y(T)}, \tag{53}$$

with

$$X(T) = \gamma^b(s_{crit}, T) K_{sites}(\gamma_{pass} + 2)\gamma_{vol}, \tag{54}$$

$$Y(T) = 8I(T)\phi g_{\mathrm{C}}^{at}(\gamma_{pass} + 1), \tag{55}$$

where $I(T)$ stands for the integral over bond states,

$$I(T) = \int_{s=0}^{s_{crit}} \gamma^b \gamma_{vol} ds/d = \int_{s=0}^{s_{crit}} e^{-E_{cb}s/Ts_{crit}} \gamma^\mu \gamma_{vol} ds/d$$

$$= \frac{Ts_{crit}}{E_{cb}d} + O(T^2), \tag{56}$$

which goes linearly to zero, while $\gamma^b(T) \propto e^{-E_{cb}/T}$ vanishes for $T \to 0$ faster than any power of T. Hence $X/Y \to 0$ so that Eq. (53) implies

$$\lim_{T \to 0} K = K_{sites} \tag{57}$$

as conjectured.

This low temperature limit ($T \ll E_{cb}$) is of general interest since it represents a sticky gas of ideal spheres, which serves as a model for aggregation in various areas of physics [51] and astrophysics [52]: Once two particles had contact, the remaining degree of freedom is tangential motion. The analytic prediction of formula (51) is $K_{sites} = 4$ in the limit of exact contacts, $s_{crit} = 0$. In order to evaluate Eq. (50) for positive s_{crit} we insert the near-contact decay γ^μ given by the general results (10), (14), and (32), setting $D = 2$. The explicit expression for γ^μ which we use throughout this article for results without free parameters is given in Appendix B. Here we take into account known formulas for the contact value g_{C}^{at} at low densities, as well as higher corrections to the free volume theory. Inserting this expression in Eq. (50) results in the curve shown in Fig. 9. We have performed simulations in this low-temperature limit. The wet granular matter was initially prepared in a gas state with $T = 50E_{cb}$ and cooled by the formation and rupture of bonds. The insets in Fig. 9 show final states when the granular temperature T is more than one order of magnitude below E_{cb} and no further change in the configuration was observed on exponential time scales. The symbols in Fig. 9 have been measured in this final state. In perfect agreement with the prediction of Eq. (51), we find in the contact limit, $s_{crit} \to 0$, the coordination to be exactly 4. Moreover, the increase in the number of bonds per particle with the increase of the maximal bridge length s_{crit} is found to be in very good agreement with the simulations.

Further analytic results for high densities are shown in Fig. 10(a). As is intuitively clear and shown by the family of curves in Fig. 10(a), the convergence of the limit $s_{crit} \to 0$ is not uniform with respect to density, since K_{sites} is pinned to the kissing number 6 of the monodisperse crystal density at ϕ_{max}.

IV. EQUATION OF STATE

We are now in the position to derive the equation of state, $P = P(T, \phi)$, for wet granular matter with capillary bonds tensile up to the rupture length s_{crit}. The cohesion of capillary bridges will reduce the pressure as compared to a dry hard-sphere system of equal temperature. By virtue of Eq. (53), we have the bridge coordination number K as a function of density ϕ and granular temperature T. Since in the minimal capillary model [10] the bridge force is assumed to be independent of the bridge length s, the knowledge of the mean number of bridges K will allow us to evaluate the reduction of the pressure due to cohesion. Furthermore, the particle-particle collisions are enhanced by the bridge attraction, increasing the contact correlation. The contact correlation g_{C}^{wet} for wet granular matter derives from Eqs. (45) and (46):

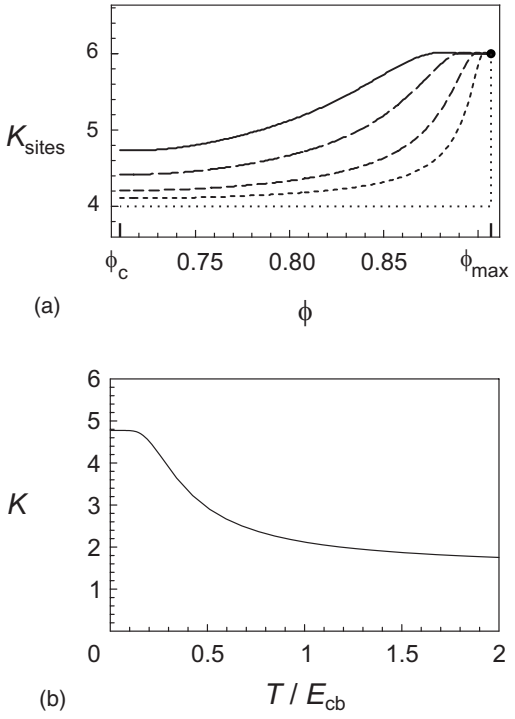

FIG. 10. (a) Maximum number of "docking sites" for capillary bonds on a particle, K_{sites}, which is possible in two dimensions given the pinch-off length s_{crit} of capillary bridges and the density ϕ. K_{sites} is independent of the temperature because it is a pure geometric quantity: the number of possible neighboring sites. Here K_{sites} is shown as a function of ϕ for different s_{crit} ranging from $s_{crit}/d=0.07$ (solid curve), 0.04, 0.02, to 0.01 (short dashes). As is shown in the text, K_{sites} is the coordination number in the zero temperature limit. While the mean coordination number K rapidly goes to zero with density for finite temperature, the zero-temperature limit is $\geqslant 4$ for all densities, because the system clusters. The dotted curve represents the limit $s_{crit} \to 0$. The longer s_{crit} the closer K_{sites} comes to six, the number of next neighbors in two dimensions. In the limit $s_{crit} \to 0$ the coordination K_{sites} converges to the number of exact contacts which is precisely four. (b) The capillary bridge coordination K drops down in the vicinity of the critical temperature as clustered structures break up. For this plot the mean density is chosen to be $\phi=0.75$.

$$g_{\copyright}^{wet} = g_{\copyright}^{at} \frac{(1+\gamma_{pass})(1+\gamma^{b}\gamma_{vol})I^{u}}{(1+\gamma_{pass}-\gamma^{u}\gamma_{vol})I^{b}+(2+\gamma_{pass})\gamma^{b}\gamma_{vol}I^{u}} \quad (58)$$

with the integrals

$$I^{u/b} = \int_{0}^{s_{crit}} \gamma^{u/b}(s)\gamma_{vol}(s)ds. \quad (59)$$

The analytic expression (58) for the contact correlation of wet granular matter, $g_{\copyright}^{wet}$, is indeed strictly greater than the one of the dry system, $g_{\copyright}^{at}$, to which it converges in the high temperature limit when the capillary energy E_{cb} is small compared to the granular temperature T. This limit follows obviously from Eq. (58) because the functions with superscript index "b" turn into those with "u" for $T \gg E_{cb}$. In the low temperature limit, liquid bonds oscillate with an amplitude proportional to the kinetic energy which equals T on average, so that the probability to find the particles at contact, $g_{\copyright}^{wet}$, grows proportional to $1/T$, as can be derived easily from Eq. (58) using the expansion (56).

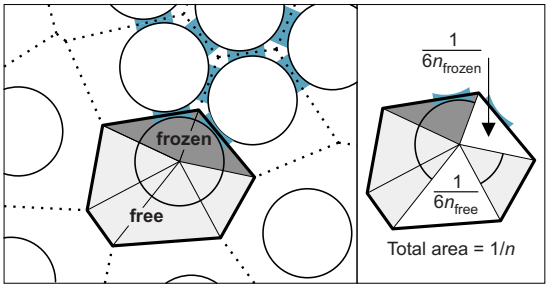

FIG. 11. (Color online) A local configuration of two-dimensional wet granular matter at moderate density. The cell borders are located at one half of the surface separation for polydisperse diameters (not half center distance), so that each cell contains one particle completely. Since there is one particle in each Voronoï cell, the mean area equals the inverse density. In Sec. II A we have used the Voronoï tessellation to compute the derivative of the pair correlation at contact for a dry and dense system. For such a dense system, the Voronoï cell resembles a hexagon with a size proportional to $(d+s)^2$, where s is the particle separation. In wet granular matter, we distinguish the densities n_{free} and n_{frozen} associated with the binding status of the capillary interaction. A stable capillary bond contributes $1/(6n_{frozen})$ to the cell area, $1/n$, and thus less than an unconnected neighborhood with $1/(6n_{free})$ does. The areas sum up to the cell size, so that these densities are related as expressed by Eqs. (61) and (62).

A. Frozen degrees of freedom

As the system starts to cluster at temperatures close to E_{cb}, voids remain between the clusters with linear dimensions large compared to the particle diameter. Clearly, this growing length scale, which is set by the sizes of clusters and voids, is not captured by the short-range behavior of the pair correlation function. Here we advance the theory beyond the level of two-particle correlations to take correlation on large scales, such as the collective particle motion in a cluster, in an approximative fashion into account.

The collective motion of a cluster is due to stable capillary bonds which impose constraints, such that the internal degrees of freedom of clusters are frozen. Since K is the number of instantaneous capillary bridges of which the fraction $\mathrm{erf}(\sqrt{E_{cb}/T})$ with kinetic energies below E_{cb} forms stable bonds, we have

$$K_{frozen} = K\,\mathrm{erf}\left(\sqrt{\frac{E_{cb}}{T}}\right) \quad (60)$$

for the number of frozen degrees of freedom.

We are interested in the density of the remaining degrees of freedom. The idea is simple and powerful: As a general mathematical property of triangulations, there are on average precisely six Voronoï neighbors [42], independent of density or ordering. In Fig. 11 we can observe that the Voronoï neighbors with stable bonds contribute less to the area $1/n$ of

the Voronoï cell. This picture suggest a two-fluid model with frozen and free neighborhoods as the two constituents. The fraction of frozen and free triangulation bonds is proportional to K_{frozen} and K_{free}, respectively, and the area contributions associated to each bond sum up to the total size of the Voronoï cell:

$$K_{\text{frozen}} + K_{\text{free}} = 6, \tag{61}$$

$$\frac{K_{\text{frozen}}}{n_{\text{frozen}}} + \frac{K_{\text{free}}}{n_{\text{free}}} = \frac{6}{n}. \tag{62}$$

Because of this reciprocal sum rule for the densities one may call this a reciprocal two-fluid model. The densities $n_{\text{free}} < n < n_{\text{frozen}}$ introduced by Eq. (62), generalize the mean density n by decomposing the volume $1/n$ per particle into bound and free neighborhoods on the mean-field level. $1/(6n)$ is the average volume of a neighborhood, since there are six neighborhoods on average. The contribution of a free Voronoï neighbor is $1/(6n_{\text{free}})$, and $1/(6n_{\text{frozen}})$ is the contribution of a neighborship frozen by a capillary bridge. Put in physical terms, n_{frozen} is the local density inside a cluster.

The density n_{frozen} of the stable bond component follows analogously to Eq. (2) when averaged with the additional exponential factor (52) due to the capillary force:

$$\left\langle \left(1 + \frac{s}{d}\right)^D \right\rangle_{\text{frozen}} = \frac{n_J}{n_{\text{frozen}}}, \tag{63}$$

$$\langle \cdots \rangle_{\text{frozen}} = \frac{\int_0^{s_{\text{crit}}} \cdots \gamma_{\text{frozen}}(s)\gamma_{\text{vol}}(s)ds}{\int_0^{s_{\text{crit}}} \gamma_{\text{frozen}}(s)\gamma_{\text{vol}}(s)ds}, \tag{64}$$

$$\gamma_{\text{frozen}}(s) = \exp\left\{ -\phi g_{\text{©}}^{\text{at}} \left[\left(1 + \frac{s}{d}\right)^D - 1 \right] - \frac{E_{\text{cb}}}{T} \frac{s}{s_{\text{crit}}} \right\}. \tag{65}$$

Without affecting the leading order in s/d one is free to replace the last s in the exponent (65) by $s + s^2/(2d)$, so that the integral (63) is elementary resulting in

$$\frac{n_J}{n_{\text{frozen}}} - 1 = \left[\left(1 + \frac{s_{\text{crit}}}{d}\right)^D - 1 \right] \left(\frac{1}{\alpha} - \frac{1}{e^\alpha - 1} \right), \tag{66}$$

$$\alpha = \left[\left(1 + \frac{s_{\text{crit}}}{d}\right)^D - 1 \right] \left(\phi g_{\text{©}}^{\text{at}} + \frac{E_{\text{cb}}}{T} \frac{d}{D s_{\text{crit}}} \right). \tag{67}$$

We point out that Eq. (66) implies Eq. (4) in [17] for $D=1$.

From the Eqs. (53), (60)–(62), (66), and (67) follows the density of degrees of freedom which are not frozen out by capillary bonds, $n_{\text{free}}(T, s_{\text{crit}}, \phi)$. One may regard n_{free} as the density of clusters.

We remark that the two-fluid model of neighborhoods is the only concept presented in this theory of wet granular matter which cannot be generalized in a straightforward manner to three dimensions, because for $D=3$ the number of Voronoï neighbors is not a universal constant (such as 6 for $D=2$ and 2 for $D=1$), but depends on the granular order (reaching its minimum value 12 for close packing and its maximum of approximately 15.5 in the ideal gas limit) [53]. The reason for this is that three-dimensional space cannot be filled with tetrahedrons, while flat space can be tiled by triangles. As a consequence, the number of constituents in the two-fluid model of neighborhoods would not be conserved for $D=3$ and the numerator on the right-hand side of Eq. (62) is not a constant.

B. Pressure of wet granular matter

Here we arrive at the pressure $P(T, \phi)$ using the density $n_{\text{free}}(T, \phi)$ (61) of degrees of freedom, the coordination $K(T, \phi)$ (53), and the contact correlation $g_{\text{©}}^{\text{wet}}(T, \phi)$ (58). The pressure is the trace of the stress tensor

$$P = -\frac{1}{D} \text{tr} \underline{\underline{\sigma}}. \tag{68}$$

The stress tensor $\underline{\underline{\sigma}} = \underline{\underline{\sigma}}^{\text{kin}} + \underline{\underline{\sigma}}^{\text{force}}$ describes the flow of momentum. The kinetic term has components $\sigma_{i,j}^{\text{kin}} = -\Sigma_k^N \langle m v_i^{(k)} v_j^{(k)} \delta(\mathbf{r} - \mathbf{r}^{(k)}) \rangle$. With the granular temperature $T = \langle m v_i v_i \rangle$, its trace yields nT for uncorrelated particle motion (as in an ideal gas). In general we have the kinetic contribution

$$P^{\text{kin}} = n_{\text{free}} T, \tag{69}$$

wherein there frozen degrees of freedom have been taken out. For moderate densities, one may interpret Eq. (69) as the kinetic contribution to the pressure due to a gas of clusters.

The interparticle forces $\mathbf{F}$ give rise to the Cauchy tensor $\underline{\underline{\sigma}}^{\text{force}}$, which is the tensor product of the center-to-center vector $\mathbf{r}$ and the pair force $\mathbf{F}$,

$$\underline{\underline{\sigma}}^{\text{force}} = \frac{n_{\text{free}}}{2} \langle \mathbf{F} \otimes \mathbf{r} \rangle, \tag{70}$$

so that $\underline{\underline{\sigma}}^{\text{force}}$ is diagonal for radial forces. The factor $1/2$ assigns half of the momentum current to either of the interaction particles, i.e., $\mathbf{r}/2$ may be seen as the transport vector within the Voronoï cell. The Cauchy tensor (70) has contributions only by the unfrozen pairs of particles with density n_{free}, because in frozen neighborhoods the repulsive momentum exchanged in collisions is exactly balanced by the bridge attraction under the time average on the right-hand side of Eq. (70).

A comment on the significance of the reciprocal two-fluid model as represented by Eqs. (61) and (62) is in order here. We consider for instance a compressed state of wet granular matter with K_{frozen} around five and K_{free} around unity. While K_{free} is small, the prefactor n_{free} in Eq. (70) is not necessarily small. From Eqs. (61) and (62) follows that both, n_{free} and n_{frozen}, converge to n_J as the system gets jammed ($n \to n_J$), so that the repulsive dominated state is correctly described by the Cauchy tensor (70) which grows beyond all bounds as $n \to n_J$. If one had (in contradiction to the additivity of areas) summed up densities linearly instead of the reciprocal sum rule (62), the free density would vanish or could even become negative under such conditions.

It is finally easy to determine the time average on the right-hand side of Eq. (70) for the two different forces acting in wet granular matter, the delta force in collisions of hard particles and the flat force $F_{\rm cb}=E_{\rm cb}/s_{\rm crit}$ of the capillary bonds. In a collision at time $t_{\rm coll}$ the radial momentum $\Delta\mathbf{p}$ is transferred instantaneously:

$$\begin{aligned}\langle \mathbf{F}_{\rm coll} \otimes \mathbf{r}\rangle &= \langle \Delta\mathbf{p} \otimes \mathbf{r}\,\delta(t-t_{\rm coll})\rangle \\ &= \mathbb{1}\langle \Delta p(\mathbf{r},-\mathbf{v})\,\theta[(\mathbf{r},-\mathbf{v})]\delta(r-d)\rangle \\ &= -\mathbb{1} g_{\rm C}^{\rm wet} n\sigma_D d^D T. \end{aligned} \tag{71}$$

In the last equality the δ function gives rise to the contact correlation $g_{\rm C}^{\rm wet}$ and the trivial integration of angles leaves $\sigma_D d^{D-1}$. $\mathbb{1}$ is the unity matrix and θ is the Heaviside step function. Inserting Eq. (71) in Eq. (70) and taking the trace (68) yields

$$P^{\rm coll} = 2^{D-1} n_{\rm free} T \phi g_{\rm C}^{\rm wet}. \tag{72}$$

The cohesive virial due to capillary bridges is

$$\langle \mathbf{F}_{\rm cb} \otimes \mathbf{r}\rangle = \left\langle K\frac{E_{\rm cb}}{s_{\rm crit}}\frac{\mathbf{r}\otimes\mathbf{r}}{r}\right\rangle = \frac{\mathbb{1}}{D}K\frac{E_{\rm cb}}{s_{\rm crit}}\langle d+s\rangle \approx \frac{\mathbb{1}}{D}K\frac{E_{\rm cb}}{s_{\rm crit}}d. \tag{73}$$

Hence the final result

$$P = n_{\rm free}T(1+2^{D-1}\phi g_{\rm C}^{\rm wet}) - n_{\rm free}E_{\rm cb}\frac{K}{2D}\frac{d}{s_{\rm crit}}, \tag{74}$$

where the last term is the bridge cohesion (73). Since $n_{\rm free}$, the contact correlation $g_{\rm C}^{\rm wet}$ and K have been derived explicitly in Eqs. (61), (58), and (53) as functions of ϕ and T, we have the equation of state for wet granular matter, $P=P(\phi,T)$.

Figures 12 and 13 show the analytic result (74) as a function of the granular temperature T and the density ϕ. In the high temperature limit wet granular matter behaves as a hard-spheres system. Below the critical point granular clusters are predicted to segregate due to the mechanically unstable branch of the pressure as a function of density, which appears in Fig. 13 below the critical temperature. Figure 14 provides a closeup of the critical point of wet granular matter and its spinodal. The critical density of this transition is high, because the particles have to be close enough in order to form a dynamical capillary network. As we show in Fig. 15, the critical density is determined by the length scale of capillary bridges, such that the rupture length $s_{\rm crit}$ scales with the mean particle separation $\bar{s}$. Moreover, the rupture length is approximately four times the mean particle separation, $s_{\rm crit}\approx 4\bar{s}$ (dashed line shown in Fig. 15 for comparison). This result is to be compared with the very same ratio for the reported critical density of the unclustering effect [17]: In the free cooling of dense one-dimension wet granular matter, the granular network was found to break up into granular droplets which precipitate out of the homogenous intial state, as soon as the density exceeded a critical value. This critical density was shown numerically and analytically to be set by $s_{\rm crit}\approx 3\bar{s}$ [17]. The different prefactor is due to the additional cooling dynamics and the dimensionality $D=1$. The theory

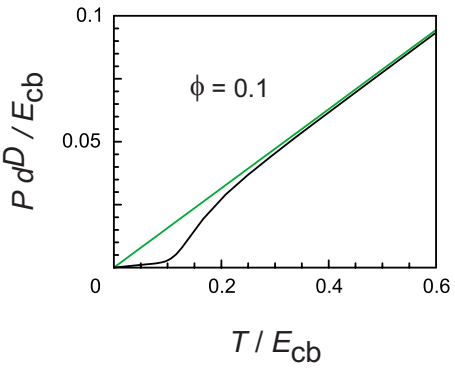

FIG. 12. (Color online) The pressure P of wet granular matter is shown as function of the granular temperature T. The dimensionality is $D=2$ and the covered area fraction is $\phi=0.1$, so that at high temperatures the system is a dilute gas. The maximum bridge length is $s_{\rm crit}=0.07d$. The behavior below the critical temperature $T_c=0.274E_{\rm cb}$ of wet granular can be understood in the following way: The system agglutinates to clusters. With these effective particles the pressure is reduced according to the reduced number density of effective particles. The breakup of clusters is reflected by the rising pressure around T_c. The straight line is the athermal pressure of hard disks, $P^{\rm dry}=ng_{\rm wall}^{\rm at}T$ which is reached asymptotically when the granular temperature is higher than the energy scale $E_{\rm cb}$ set by the capillary interaction.

of wet granular matter presented in this work predicts this transition to persist in higher dimensions.

As we shorten the rupture length $s_{\rm crit}$ (which can be easily done experimentally by evaporating the wetting liquid), the dry system is approached in such a way that the spinodal narrows in the $T-\phi$ plane and is shifted to the jamming point, where it eventually shrinks to a line and vanishes. Figure 15 shows the convergence of the critical density to the jamming density. Since the capillary bridge regime sets an upper limit on the rupture length, the critical point is con-

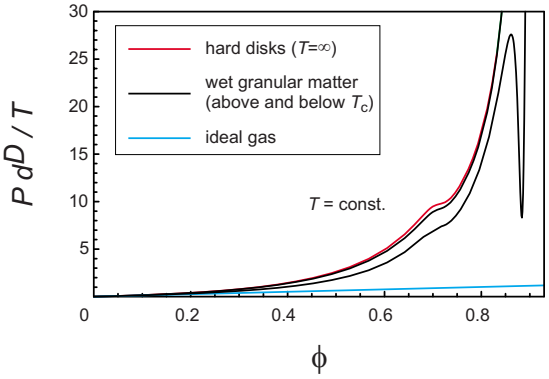

FIG. 13. (Color online) Isotherms of wet granular matter for the realistic rupture length $s_{\rm crit}=0.07d$. In the high temperature limit the liquid bridges forfeit their influence on the dynamics, so that the equation of state reduces to the hard sphere pressure. This can be seen by the two black isotherms of wet granular matter, of which the higher is at $T=E_{\rm cb}$ and converges to the top curve in the limit $T\gg E_{\rm cb}$. The lower black isotherm is at $T=0.2E_{\rm cb}$ and exhibits an unstable branch. The critical point is at $T_c\approx 0.274E_{\rm cb}$ (cf. Fig. 14 for a closeup).

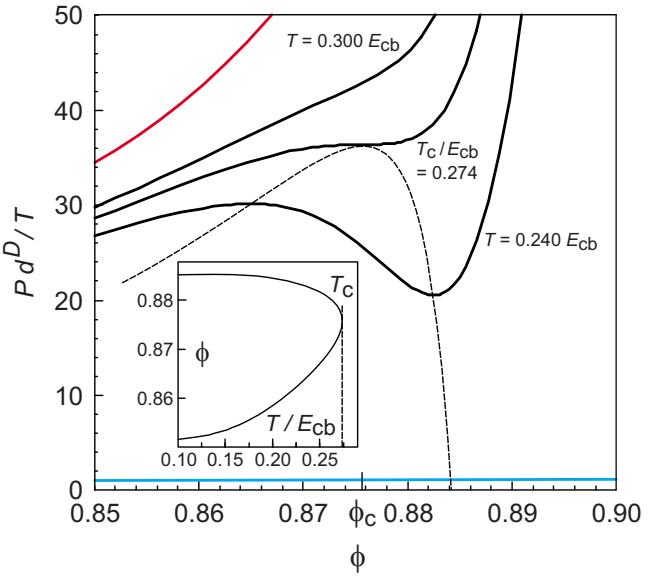

FIG. 14. (Color online) A closeup of the transition region in wet granular matter. The dashed line in the main panel is the spinodal of the homogeneously driven wet granular system in $D=2$ dimensions. The solid black lines are wet granular isotherms around the critical point, which is located at $T_{\mathrm{crit}}=0.273(5)E_{\mathrm{cb}}$ for $s_{\mathrm{crit}}=0.07d$. The change of the critical point with the amount of added liquid (represented by s_{crit}) is shown in Fig. 15. The curve in the upper left corner is the athermal pressure P^{dry} of the hard disk system [31] without liquid bridges, and the line at the bottom is the ideal gas pressure [$P^{\mathrm{id}}=d^D(\phi)$ has a defined slope]. $P^{\mathrm{dry}}=g_{\mathrm{C}}^{\mathrm{at}}P^{\mathrm{id}}$ is increased compared to the ideal gas by the Enskog factor $g_{\mathrm{C}}^{\mathrm{at}}$. The pressure of wet granular matter is reduced compared to the dry system P^{dry} due to the capillary cohesion. The inset shows the spinodal in the temperature-density plane, where the critical temperature can be clearly determined.

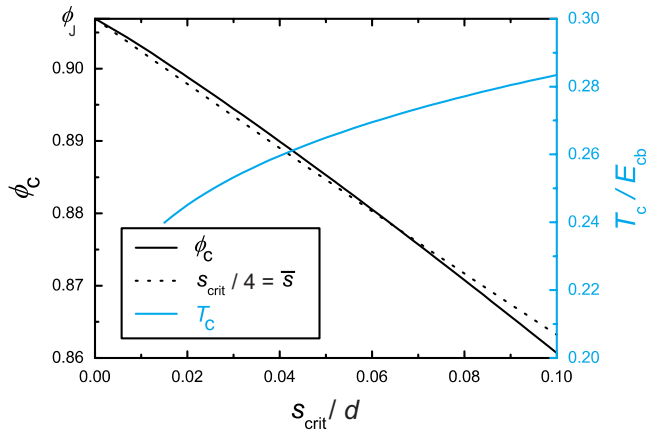

FIG. 15. (Color online) The influence of the rupture length s_{crit} on the position of the critical point in the phase diagram Fig. 14 of wet granular matter. The position of the critical point is described by the critical parameters $(\phi_{\mathrm{c}},T_{\mathrm{c}})$, which are plotted on the left and right vertical axis, respectively. Solid lines result from the full theory (74) by solving for the intersection of $\partial_\phi P(\phi,T)=0$ and $\partial_\phi^2 P(\phi,T)=0$. For the critical temperature we find a very mild variation with the rupture length, so that over the entire physically relevant range of capillary interaction we have $T_{\mathrm{c}}\approx E_{\mathrm{cb}}/4$. The influence of the rupture length s_{crit} on the critical density ϕ_{c} can be understood very clearly with the help of the dashed line. The dashed line is the implicit equation $s_{\mathrm{crit}}=4\bar{s}(\phi)$ for the density ϕ, which is expressed in terms of the mean particle separation $\bar{s}(\phi)=d(\sqrt[D]{\phi_J/\phi}-1)$. Since the dashed line closely follows the full theory, the critical density is such that the mean particle separation scales with the rupture length s_{crit}. This shows that both intrinsic characteristics of the capillary interaction, the rupture length and the bridge energy E_{cb}, determine the critical point of wet granular matter.

fined on the density axis between the ordering transition at ϕ_{o} and the jamming density ϕ_{J}. The critical temperature almost exclusively depends on the bridge energy, according to $T_{\mathrm{c}}\approx E_{\mathrm{cb}}/4$, over the entire capillary regime.

With this discussion of transitions occurring in wet granular matter the presentation of our theory for wet granular matter is completed. The reader may find in Appendix C a brief methodical extension of the theory where a self-consistent equation is derived for future works.

V. CONCLUSION

Starting with the hard-sphere fluid, an expression (10) for the narrowing of the near contact pair correlation was derived, which describes in the jamming limit the delta peak of $2D$ isostatic contacts per particle, in agreement with the accepted value of simulations. In the gas and fluid regime the fall-off predicted by this expression for the pair correlation at contact was found to be well confirmed by simulations. We then addressed the nonequilibrium case of wet granular matter by the introduction of capillary bridges which are formed hysteretically. The description in terms of the pair-correlation function was extended with six different nonvanishing correlation coefficients which take the bridge status into account and allow for the hysteretic dissipative dynamics. The coordination number of bonds was computed analytically as a function of the rupture length of the capillary bridges, the granular temperature, and the density. The limiting case of strong bonds led to the sticky gas dynamics for which simulations have been performed which showed very good agreement with the analytic prediction of the coordination number. Based on the derived expressions for the contact correlation and the bridge coordination, we finally computed the pressure of wet granular matter analytically as a function of density and granular temperature. Here a method was put forward, which describes the effective degrees of freedoms in order to take the correlated motion of particles glued to clusters into account. The isotherms of wet granular matter were found to have an unstable branch which gives rise to the segregation of dense clusters. The critical temperature of this transition was derived to be approximately one quarter of the capillary bond energy. The critical density is directly related to the pinch-off distance of the capillary bridges. A close relation to the unclustering effect reported in one dimension [17] was shown, for which reason this effect persists also in higher dimensions.

It will be interesting to probe the critical point of wet granular matter experimentally and by direct simulations. As

we have shown, the position of the critical point is determined by the length and energy of the capillary bridges. These quantities can be controlled very accurately in an experiment of shaken wet granular matter. Therefore the measurement of the critical temperature will allow to discern between extensions such as the nonlinear coupling discussed in Appendix C.

Future analytic work includes the background contribution g_B in the dense regime, since our numerics indicate that the pair correlation is flatter near the contact as predicted by g_A alone. This task might be addressed in conjunction with the analogous background contribution in three dimensions, for which in the jamming limit an integrable power-law divergence, $g_B \propto 1/s^\delta$, has been reported in numerical studies (with $\delta=0.5$ [54] or $\delta=0.6$ [34]) and experiments [55], but is as well lacking a theoretical explanation at present.

ACKNOWLEDGMENTS

Discussions with Martin Brinkmann, Svenja Hager, Jürgen Vollmer, Klaus Röller, and Mario Scheel are gratefully acknowledged.

APPENDIX A: THE BACKGROUND CONTRIBUTION g_B

1. Weighting factors

With g_A in Eq. (10) we considered the four [cf. Eq. (12)] A neighbors, which form isostatic contacts at jamming, $s_A \to 0$ for $\phi \to \phi_J$ (3), and are separated by s_A according to Eq. (4) before jamming. Analogously, the separation s_B of the two B neighbors is weighted by

$$P_B(s_B) \propto \exp\left(-\frac{\left(1+\frac{s_B}{d}\right)^2-1}{\phi_{max}/\phi-1}\right). \tag{A1}$$

While in Eq. (4) the denominator in the exponential is $c_A = \phi_J/\phi - 1$ so that $s_A \to 0$ at the jamming density, in Eq. (A1) the denominator is $c_B = \phi_{max}/\phi - 1$ since the blocked B is only forced to form a contact, $s_B \to 0$, for a perfect crystal with $\phi \to \phi_{max}$. Of course, this limit is kinematically unreachable because the system comes to rest at the jamming density $\phi_J < \phi_{max}$. ϕ_{max} would be reached. We note that c_B is a small dimensionless quantity: For $\phi > \phi_o = 0.71$ we have $0 < c_B < 0.2774$.

Close to jamming, the B neighbors are fixed in space by particles other than the reference particle. Except for arch-like constructions which are rare for frictionless particles, and would include second Voronoï neighbors keeping B at a separation larger than our region of interest, $s_B > s_{crit}$, this hindrance is due to the A neighbors. Therefore the probability $g_B(s_B)$ to find a B neighbor at separation s_B from the reference particle (sketched with hatching in Fig. 17) is given by the integral over all configurations where four A neighbors hinder two B neighbors.

The configurations will be weighted by a phase space factor C and the exponential factor P_B. We are above the ordering density ϕ_o, so that the neighborhood has (by definition of the phase) hexagonal order as sketched in the inset of Fig. 16. Projecting the configurations with the two B neighbors blocked (gray subset in Fig. 16) on a single θ axis, we find the configuration space factor

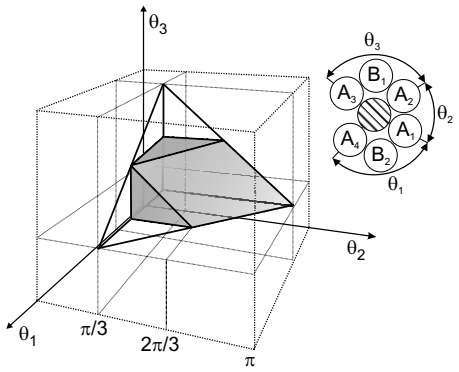

FIG. 16. The angular configuration space of four neighbors close to the reference particle. These we denote as A neighbors. The faceted inner subset shown in gray is the subspace conditioned to the property that two further particles, the B neighbors, are hinder by the A particles in approaching the reference particle. The projection of this subset onto an θ axis (for the angle between a blocking A pair, θ_1 or θ_3 in this example) gives rise to a linear configuration space factor $C(\theta)$. Obviously a B neighbor acts like a wedge driven between two A neighbors, and therefore increases θ. This is taken into account by the weighting factor $P_B(s_B)$ which favors shorter separations s_B between the particle B and the reference particle, depending on the density ϕ.

$$C(\theta) = \frac{3(5\pi - 6\theta)}{2\pi^2}. \tag{A2}$$

In the sequel we abbreviate

$$\gamma_{vol}(s) \propto 1 + s/d. \tag{A3}$$

for the volume factor (A1) in $D=2$. Wide gaps of length s_B are exponentially suppressed by P_B.

2. Configuration space

Let us now address the configuration space plotted in Fig. 17. If the opening angle θ of the A neighbors exceeded $\theta_T(s_A)$,

$$\cos\frac{\theta_T(s_A)}{2} = \frac{\sqrt{s_A(2d+s_A)}}{d+s_A}, \tag{A4}$$

the B particle could slip through and turn into an A neighbor, which is defined by having a free path towards the reference particle. This transition corresponds to the neck connecting different jamming island in the configuration space. Only along the line ($\overline{PQ}$ in Fig. 17) defined by $\theta = \theta_c(s_A)$,

$$\cos\frac{\theta_C(s_A)}{2} = \frac{s_A + d}{2d}, \tag{A5}$$

the B neighbor can touch the reference particle, so that $s_B = 0$. Equations (A4) and (A5) define the upper boundary of the domain of integration for all s_A,

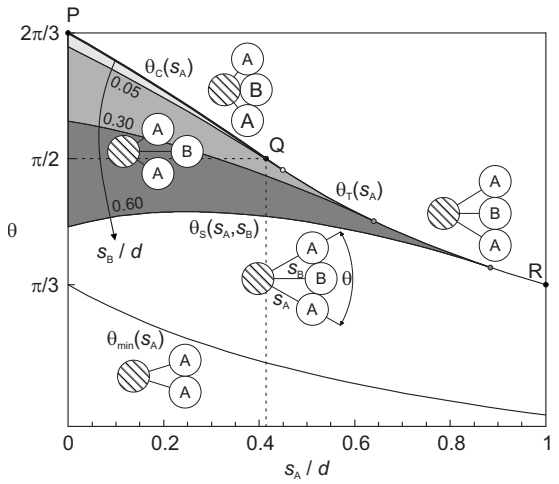

FIG. 17. A section of the configuration space of neighboring particles. Within the gray domain the particle denoted by B is blocked: The two neighbors labeled A sterically hinder the particle B from approaching the reference particle (shaded). Only at the boundary $\theta_C(s_A)$ (curve $\overline{PQ}$ ranging from $[s_A,\theta]_P=[0,2\pi/3]$ to $[s_A,\theta]_Q=[(\sqrt{2}-1)d,\pi/2]$) can the B neighbor touch the reference particle. The probability $g_B(s_B)$ to find a B neighbor at a separation s_B follows from integrating over the gray domain, which grows with increasing s_B. The lower bound, $\theta_S(s_A,s_B)$, is plotted for the values $s_B=0.05$, 0.30, and 0.60. Large areas spanned by this neighborhood are exponentially rare the higher the mean density ϕ, so that the probability distribution in this plot concentrates in the vicinity of the upper left corner P as we come closer to the jamming limit. At the line $\overline{QR}$ the B neighbor slips through and turns into an A neighbor, so that $\overline{QR}$ is the transit to another jamming island in configuration space. The corresponding transition rate is proportional to the probability density along $\overline{QR}$ and therefore vanishes in the jamming limit.

$$\theta_{\max}(s_A)=\begin{cases}\theta_C(s_A), & s_A/d\leqslant\sqrt{2}-1,\\ \theta_T(s_A), & s_A/d\geqslant\sqrt{2}-1,\end{cases} \tag{A6}$$

which is continuously differentiable but not smooth at the point Q.

The lower boundary is

$$\cos\frac{\theta_S(s_A,s_B)}{2}=\frac{(s_A+d)^2+s_B^2+2ds_B}{2(s_A+d)(s_B+d)}, \tag{A7}$$

where B hits A.

The simple lower bound on θ,

$$\cos\frac{\theta_{\min}(s_A)}{2}=\sqrt{1-\left(\frac{d/2}{d+s_A}\right)^2}, \tag{A8}$$

which ensures that the A neighbors do not overlap is without applicatory relevance, as it implies that the B neighbor is pushed out to $s_B/d>\sqrt{3}-1\approx 0.73$. This is suppressed in the dense regime $\phi>\phi_o$ by the factor F of Eq. (A1).

The configuration space ends to its right in a cusp where the lower and upper bound intersect at

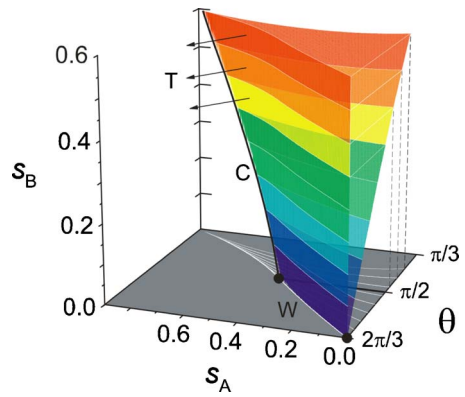

FIG. 18. (Color online) s_A-θ plot of Fig. 17 with the full s_B dependence shown on the additional vertical axis.

$$s_A^{\text{cusp}}(s_B)=\sqrt{s_B^2+2ds_B+2d^2}-d. \tag{A9}$$

This cusp converges to the point Q for $s_B\to 0$.

With the integration bounds (A6), (A7), and (A9), and the weighting factors (A1) and (A2) we have

$$g_B(s_B)=\mathcal{N}P_B(s_B)\times\left[\int_0^{s_A^{\text{cusp}}(s_B)}ds_A P_A(s_A)\gamma_{\text{vol}}(s_A)\int_{\theta_S(s_A,s_B)}^{\theta_{\max}(s_A)}d\theta C(\theta)\right]^2 \tag{A10}$$

$$=\mathcal{N}P_B(s_B)\left[\frac{s_B}{d}I_1(n)+\left(\frac{s_B}{d}\right)^2 I_2(n)+O\left(\left(\frac{s_B}{d}\right)^3\right)\right]^2. \tag{A11}$$

We emphasize that the configuration space (s_A,θ) describes the relative position of one A-neighbor sketched symmetrically in Fig. 17 (see also Fig. 18). Since there are two independent A neighbors involved, their configuration is the direct product $(s_{A1},\theta_1)\times(s_{A2},\theta_2)$. On this account the configuration integral is squared in Eq. (A10), with the important consequence that the leading order in $g_B(s_B)$ is quadratical. The normalization constant $\mathcal{N}$ is determined by the knowledge that there are two B neighbors. While the exponential prefactor dominates the long range decay, we expand the near-contact increase in s_B/d. Substituting the dimensionless area $z_A=([1+s_A/d)^2-1]/c_A$ for integration in favor of the particle separation s_A, the expressions I_i, $i=1,2$ are of the form

$$I_i=c_A\int_0^{1/c_A}e^{-z_A}f_i(c_A z_A)dz_A, \tag{A12}$$

with

$$f_1(x)=\frac{3(x-1)\alpha(x)}{2\pi^2\sqrt{(3-x)(x+1)}}, \tag{A13}$$

$$\frac{f_2(x)}{f_1(x)}=\frac{2}{x-3}-\frac{2}{x-1}+\frac{6\sqrt{x+1}}{\alpha(x)\sqrt{3-x}}-\frac{6\sqrt{3-x}}{\alpha(x)\sqrt{x+1}}-1,$$

$$\alpha(x) = \pi - 12 \arcsin \frac{\sqrt{x+1}}{2}. \tag{A14}$$

The integrals I_i can be treated by expanding the functions $f_i = \Sigma_\nu f_i^{(\nu)} x^\nu$:

$$I_i = \sum_{\nu=0}^{\infty} f_i^{(\nu)} c_A^{\nu+1} \underbrace{\int_0^{1/c_A} e^{-z} z^\nu dz}_{=\nu! - \Gamma(\nu+1, 1/c_A)}. \tag{A15}$$

All incomplete gamma functions can be eliminated by virtue of the recurrence relation (cf. (6.5.2) and (6.5.22) in [56])

$$\Gamma(\nu+1, 1/c_A) = \nu\Gamma(\nu, 1/c_A) + (-1)^\nu c_A^{-\nu} e^{-1/c_A}. \tag{A16}$$

As is apparent from the recurrence relation, the result will be of the form

$$I_i = R_i(c_A) + e^{-1/c_A} S_i(c_A). \tag{A17}$$

The regular part, for instance in first order of s_B/d,

$$R_1(c_A) = c_A \frac{\sqrt{3}}{2\pi} + c_A^2 \frac{9 - 2\sqrt{3}\pi}{3\pi^2} + c_A^3 \frac{-27 + 2\sqrt{3}\pi}{3\pi^2} + \cdots, \tag{A18}$$

is a series expansion about the point of jamming, $c_A = 0$. It is asymptotically diverging due to the factorial which appears in the recurrence relation. Fortunately this does not restrain us from an excellent approximation, since for the relevant density, $\phi > \phi_o$, the quality of the expansion increases for more than 10 terms in the expansion [cf. panel (a) of Fig. 19]. The second part in Eq. (A17), for which the first order of s_B/d is given by

$$S_1(c_A) = c_A \frac{\sqrt{3}}{2\pi} + c_A^2 \frac{9 - 2\sqrt{3}\pi}{3\pi^2} + c_A^3 \frac{-27 + 2\sqrt{3}\pi}{3\pi^2} + \cdots, \tag{A19}$$

and has a positive radius of convergence [cf. panel (b) in Fig. 19]. This part is overexponentially suppressed by the prefactor $\exp -1/c_A$ close to jamming.

In the application to wet granular matter the subleading order $(s_B/d)^3 < 4 \times 10^{-4}$ is negligible for a realistic value of $s \leqslant s_{crit} \approx 0.07d$, whereby we have the concise result

$$g_B(s_B) = \mathcal{N} e^{-z_B} z_B^2 + O(z_B^3) \tag{A20}$$

with the abbreviation $z_B = [(1 + s_B/d)^2 - 1]/c_B$ and $1/c_B \approx \phi g_c^{at}$. The normalization $8\phi(c_B/2)\int g_B dz_B = 2$ according the two B neighbors determines $\mathcal{N}$ in Eq. (A20). Hence the result (14).

APPENDIX B: EXPLICIT EXPRESSIONS FOR THE PAIR CORRELATION IN TWO DIMENSIONS WITHOUT FREE PARAMETERS

In our general derivation of the theory of wet granular matter we distinguished between the jamming density ϕ_J and the (highest possible) crystalline packing $\phi_{max} = \pi/(2\sqrt{3})$ achieved in monodisperse domains. The exact value of the jamming density ϕ_J depends on many details such as the distribution of polydispersity and the jamming protocol for the increase of density. When we want to give explicit results without free parameters on the bridge coordination $K(T, \phi, s_{crit})$ and the equation of state $P = P(T, \phi, s_{crit})$ we do this for weak polydispersity, where the difference between ϕ_J and ϕ_{max} is negligible and the limiting case of "dry" disks has been studied extensively.

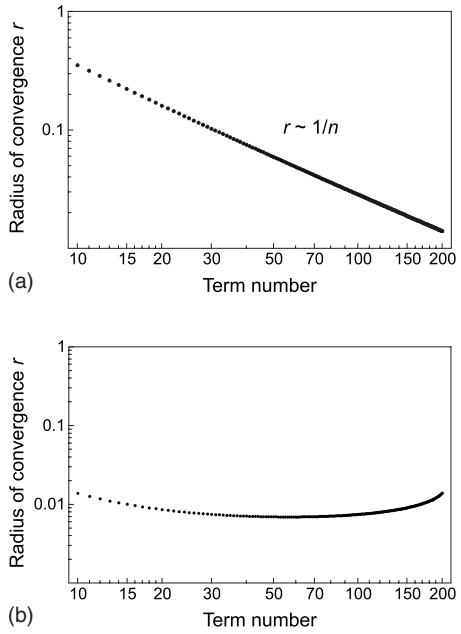

FIG. 19. The radii of convergence r_k for expansions around the jamming point. The contribution blocked B neighbors give to the pair correlation can be expanded in a series around the jamming point, $c_A = 0$. The radius of convergence is given by the Cauchy-Hadamard formula $r_j = 1/\sqrt[j]{K_j}$ for the term $K_j(s_B/d)^j$. (a) The asymptotic divergence of the R series in Eq. (A18) poses no practical problem since few terms (less than 10) give sufficient accuracy. (b) The S series in Eq. (A18) converges.

1. High density

For monodisperse "dry" disks, $\phi_J = \phi_{max}$, there are higher order corrections to the free volume result (9) available in the literature which are incorporated in the final results on the bridge coordination and the equation of state for wet granular matter. These corrections are expansions with respect to $x = \phi_J - \phi$ fitted to simulations:

$$g_c^{dense} = \left(\frac{1}{x} + a_0 + a_2 x^2 + \cdots\right)\frac{\phi_J}{\phi} = \left(\frac{1}{x} + a_0 + a_2 x^2 + \cdots\right) \times \left(1 + \frac{x}{\phi_J} + \cdots\right). \tag{B1}$$

Equation (B1) holds in the dense regime, $\phi_o < \phi < \phi_{max}$, above $\phi_o = 0.71$. The numerical coefficients are $a_0 = -1.07$ and $a_2 = 5.89$ [31], confirmed by our own simulations. Similar empirical expressions are also available for polydisperse disks in the glass state [Eq. (6) in [23]].

TABLE I. The particle-particle correlation g_c^{at} and the particle-wall correlation $g_{\mathrm{wall}}^{\mathrm{at}}$ at contact for different spatial dimensions valid up to moderate densities. The center column shows the results of the scaled particle theory and the right column contains the exact expression for one dimension, and heuristic expressions [63] of Henderson [64] for two dimensions and Carnahan-Starling [65] in three dimensions.

	Scaled particle theory		Heuristic fits	
D	g_c^{at}	$g_{\mathrm{wall}}^{\mathrm{at}}$	g_c^{at}	$g_{\mathrm{wall}}^{\mathrm{at}}$
1	$\frac{1}{1-\phi}$	$\frac{1}{1-\phi}$	$\frac{1}{1-\phi}$	$\frac{1}{1-\phi}$
2	$\frac{1-\phi/2}{(1-\phi)^2}$	$\frac{1}{(1-\phi)^2}$	$\frac{1-7\phi/16}{(1-\phi)^2}-\frac{\phi^3/128}{(1-\phi)^4}$	$\frac{1+\phi^2/8}{(1-\phi)^2}-\frac{\phi^4/64}{(1-\phi)^4}$
3	$\frac{1-\phi/2+\phi^2/4}{(1-\phi)^3}$	$\frac{1+\phi+\phi^2}{(1-\phi)^3}$	$\frac{1-\phi/2}{(1-\phi)^3}$	$\frac{1+\phi+\phi^2-\phi^3}{(1-\phi)^3}$

2. Low and moderate density

For the analytic treatment an explicit expression for the contact correlation g_c^{at} in Eq. (32) is needed [as the counterpart to the dense expression (B1)]. Aside from the trivial one-dimensional case [57], exact expressions for the contact correlation of hard spheres are unknown for the dilute regime. Yet there are well-established approximations in the literature resulting from scaled particle theory [58,59], from the virial expansions [60], as solutions of the Percus-Yevick closure [61], as well as heuristic expressions [62] such as the Carnahan-Starling formula with corrections to better fit simulation results (cf. Table I).

As in the dense regime (B1) we shall use the Henderson-Luding expression [31]

$$g_c^{\mathrm{dilute}} = \frac{1-7\phi/16}{(1-\phi)^2} - \frac{\phi^3/128}{(1-\phi)^4} \tag{B2}$$

for the uncaged regime, $0<\phi<\phi_{\mathrm{o}}$, and the merging function $m(\phi)=1/\{1+\exp[(\phi_{\mathrm{o}}-\phi)/m_0]\}$ with a crossover width $m_0=0.0111$ to smoothly connect the dense (B1) and dilute (B2) expressions [31]:

$$g(s) = m(\phi)g^{\mathrm{dilute}}(s) + [1-m(\phi)]g^{\mathrm{dense}}(s) \tag{B3}$$

with $g^{\mathrm{dilute}}(0)=g_c^{\mathrm{dilute}}$ and $g^{\mathrm{dense}}(0)=g_c^{\mathrm{dense}}$ as given by the Eqs. (B1) and (B2). The near-contact decay has been established in the Eqs. (10) and (14) for $\phi>\phi_{\mathrm{o}}$, and in Eq. (32) for $0<\phi<\phi_{\mathrm{o}}$:

$$g^{\mathrm{dilute}}(s) = g_c^{\mathrm{at}}\gamma_{\mathrm{dilute}}^{\mathrm{u}}, \tag{B4}$$

$$g^{\mathrm{dense}}(s) = g_c^{\mathrm{at}}\gamma_{\mathrm{dense}}^{\mathrm{u}} = g_c^{\mathrm{at}}\gamma_{\mathrm{dilute}}^{\mathrm{u}}\left[1+\left(\phi g_c^{\mathrm{at}}\frac{s}{d}\right)^2\right] \tag{B5}$$

up to leading order in s_{crit} with

$$\gamma^{\mathrm{u}}(s)_{\mathrm{dilute}} = \exp\left\{-\phi g_c^{\mathrm{at}}\left[\left(1+\frac{s}{d}\right)^2-1\right]\right\}. \tag{B6}$$

With the contact expressions (B1) and (B2), as well as the short-range decay formulas (10) and (32), we have sufficient information on the dry system over the entire density range. We may therefore proceed by introducing the hysteretic capillary bridges.

APPENDIX C: Self-Consistency of Bridge Coordination K

All results presented so far on the coordination $K(\phi,T)$ and pressure $P(\phi,T)$ allowed explicit analytic results. Here we want to demonstrate how to treat more complicated source terms of the hysteretic system (45) numerically. Such an extension of the theory could be motivated as follows. The current of free (unbound) approaching particles could be a function of the free density n_{free} instead of the mean density, since some of the unconnected neighbors traverse the voids between clusters, so that Eq. (41) is changed to

$$\phi g_{\textcircled{c}\leftarrow r}^{\mathrm{u}} + \phi g_{c\leftarrow\textcircled{r}}^{\mathrm{u}}/\gamma^{\mathrm{u}}(s_{\mathrm{crit}}) = (1-K/K_{\mathrm{sites}})\phi_{\mathrm{free}}g_{\textcircled{c}}^{\mathrm{at}}(\phi_{\mathrm{free}}). \tag{C1}$$

Obviously this approach is a lower estimate for the current of freely approaching particles, which is why Eq. (C1) is considered as a methodical example rather than a physical competitor to the theory presented above.

With the altered Eq. (C1) the hysteretic system (45) can still be solved analytically to find the correlation coefficients $\mathbf{g}=\{g_{\textcircled{c}\leftarrow r}^{\mathrm{u}}, g_{\textcircled{c}\leftarrow r}^{\mathrm{b}}, g_{\textcircled{c}\rightarrow r}^{\mathrm{b}}, g_{c\rightarrow\textcircled{r}}^{\mathrm{u}}, g_{c\rightarrow\textcircled{r}}^{\mathrm{b}}, g_{c\leftarrow\textcircled{r}}^{\mathrm{u}}\}$. Unlike before,

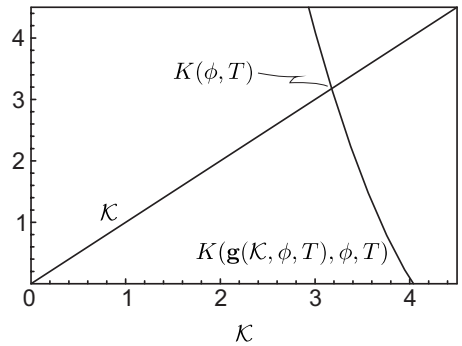

FIG. 20. Typical graphical solution of the self-consistent equation (C2). Here the density is chosen to be $\phi=0.6$ and the granular temperature is $T=0.2E_{\mathrm{cb}}$.

due to the coupling (C1) and Eqs. (60) and (61), the correlations **g** are a highly nonlinear function of K. Therefore Eq. (46) becomes a nonlinear self-consistent equation:

$$K[\mathbf{g}(\mathcal{K},\phi,T),\phi,T]=\mathcal{K}. \tag{C2}$$

The physical value $K(\phi,T)$ of the coordination is the solution $\mathcal{K}$ of Eq. (C2). The numerical solution of Eq. (C2) is found to be very robust, as Fig. 20 indicates. Plugging the resulting self-consistent $K(\phi,T)$ back into the equation for the pressure (74) of wet granular matter, we find that the critical point is shifted from $T_c=0.273(5)E_{cb}$ to $T_c=0.216(5)E_{cb}$. This reduction of the critical temperature is intuitively clear since with less particles arriving to form bonds, the wet granular matter "evaporates" at lower granular temperatures.

[1] H. Rumpf, *Agglomeration* (AIME, Interscience, New York, 1962).
[2] C. Thornton, J. Phys. D **24**, 1942 (1991).
[3] K. K. Y. C. Thornton, Powder Technol. **65**, 153 (1991).
[4] G. Lian, C. Thornton, and M. J. Adams, J. Colloid Interface Sci. **161**, 138 (1993).
[5] S. J. R. Simons, J. P. K. Seville, and M. J. Adams, *Sixth International Symposium on Agglomeration, Nagoya, Japan* (1994), p. 117.
[6] S. J. R. Simons, J. P. K. Seville, and M. J. Adams, Chem. Eng. Sci. **49**, 2331 (1994).
[7] C. Thornton, K. K. Yin, and M. J. Adams, J. Phys. D **29**, 424 (1996).
[8] G. Lian, C. Thornton, and M. J. Adams, Chem. Eng. Sci. **53**, 3381 (1998).
[9] C. D. Willet, M. J. Adams, S. A. Johnson, and J. P. K. Seville, Langmuir **16**, 9396 (2000).
[10] S. Herminghaus, Adv. Phys. **54**, 221 (2005).
[11] K. Binder, S. Sengupta, and P. Nielaba, J. Phys.: Condens. Matter **14**, 2323 (2002).
[12] C. H. Mak, Phys. Rev. E **73**, 065104(R) (2006).
[13] A. Fingerle and S. Herminghaus, e-print arXiv:0708.2597.
[14] A. Fingerle, K. Roeller, K. Huang, and S. Herminghaus, (unpublished).
[15] A. Fingerle, S. Herminghaus, and V. Y. Zaburdaev, Phys. Rev. Lett. **95**, 198001 (2005).
[16] A. Fingerle, S. Herminghaus, and V. Y. Zaburdaev, Phys. Rev. E **75**, 061301 (2007).
[17] A. Fingerle and S. Herminghaus, Phys. Rev. Lett. **97**, 078001 (2006).
[18] V. Y. Zaburdaev, M. Brinkmann, and S. Herminghaus, Phys. Rev. Lett. **97**, 018001 (2006).
[19] L. Santen and W. Krauth, Nature (London) **405**, 550 (2000).
[20] L. Santen and W. Krauth, e-print arXiv:cond-mat/0107459.
[21] M. Scheel, R. Seemann, M. Brinkmann, M. DiMichiel, A. Sheppard, B. Breidenbach, and S. Herminghaus (unpublished).
[22] We do not distinguish between the mean value and the root mean square of the diameter (relevant to the Voronoï area), because they differ only by $(\Delta d/d)^2/2<5\times10^{-3}$.
[23] A. Donev, F. H. Stillinger, and S. Torquato, J. Chem. Phys. **127**, 124509 (2007).
[24] H. Takana (private communication).
[25] Numerics reported at present [11,12] could not distinguish between a weak first order transition (with constant pressure at ϕ_O) and two subsequent continuous transitions (with slowly increasing pressure at ϕ_O).
[26] R. García-Rojo, S. Luding, and J. J. Brey, Phys. Rev. E **74**, 061305 (2006).
[27] S. Torquato, T. M. Truskett, and P. G. Debenedetti, Phys. Rev. Lett. **84**, 2064 (2000).
[28] T. Aste, J. Phys.: Condens. Matter **17**, S2361 (2005).
[29] Z. Salsburg and W. Wood, J. Chem. Phys. **37**, 798 (1962).
[30] J. Buehler, R. Wentorf, J. Hirschfelder, and C. Curtiss, J. Chem. Phys. **19**, 61 (1962).
[31] S. Luding, Phys. Rev. E **63**, 042201 (2001).
[32] R. J. Speedy, J. Chem. Phys. **100**, 6684 (1994).
[33] A. Donev, F. H. Stillinger, and S. Torquato, Phys. Rev. Lett. **96**, 225502 (2006).
[34] A. Donev, S. Torquato, and F. H. Stillinger, Phys. Rev. E **71**, 011105 (2005).
[35] T. S. Majmudar, M. Sperl, S. Luding, and R. P. Behringer, Phys. Rev. Lett. **98**, 058001 (2007).
[36] Typically one or two percent for packings produced by the Lubachevsky-Stillinger algorithm (Lubachevsky [66] for 2D, [34] for 3D).
[37] R. Connelly, http://www.math.cornell.edu/~connelly/PackingsIII.IV.pdf (2005).
[38] J.-N. Roux, Phys. Rev. E **61**, 6802 (2000).
[39] R. Connelly, Discrete Comput. Geom. **33**, 549 (2005).
[40] R. Connelly, Institut Henri Poincaré, http://www.math.cornell.edu/~connelly/BasicsI.BasicsII.pdf (2005).
[41] A. Donev, S. Torquato, F. H. Stillinger, and R. Connelly, J. Appl. Phys. **95**, 989 (2004).
[42] J. Meijering, Philips Res. Rep. **8**, 270 (1953).
[43] S. Asakura and F. Oosawa, J. Chem. Phys. **22**, 1255 (1954).
[44] S. Asakura and F. Oosawa, J. Polym. Sci. **33**, 183 (1958).
[45] J. Piasecki, L. Bocquet, and J.-P. Hansen, Physica A **218**, 125 (1995).
[46] F. M. Tao, Y. Song, and E. A. Mason, Phys. Rev. A **46**, 8007 (1992).
[47] D. Goulding and J. Hansen, Mol. Phys. **99**, 865 (2001).
[48] U. F. Edgal and D. L. Huber, Phys. Rev. E **48**, 2610 (1993).
[49] D. Henderson, D. Wasan, and A. Trokhymchuk, J. Chem. Phys. **119**, 11989 (2003).
[50] D. Henderson, A. Trokhymchuk, and D. Wasan, J. Mol. Liq. **112**, 21 (2006).
[51] R. Piazza, V. Peyre, and V. Degiorgio, Phys. Rev. E **58**, R2733 (1998).
[52] J. Blum *et al.*, Phys. Rev. Lett. **85**, 2426 (2000).
[53] T. Aste, M. Saadatfar, A. Sakellariou, and T. Senden, Physica A **339**, 16 (2004).
[54] L. E. Silbert, D. Ertaş, G. S. Grest, T. C. Halsey, and D. Levine, Phys. Rev. E **65**, 031304 (2002).
[55] T. Aste, M. Saadatfar, and T. J. Senden, Phys. Rev. E **71**,

061302 (2005).
[56] M. Abramowitz and I. A. Stegun, *Handbook of Mathematical Functions* (Dover Publications, Inc., New York, 1965).
[57] The configuration space of the one-dimensional gas is $L-Nd$, so that the equation of state is $P(L-Nd)=NT$. Comparison with the general expression $P=g_{\mathrm{wall}}^{\mathrm{at}}nT$ yields $g_{\mathrm{wall}}^{\mathrm{at}}=(1-\phi)^{-1}$.
[58] H. Reiss, H. Frisch, and J. Lebowitz, J. Chem. Phys. **31**, 369 (1959).
[59] E. Helfand, H. Frisch, and J. Lebowitz, J. Chem. Phys. **34**, 1037 (1961).
[60] F. H. Ree and W. G. Hoover, J. Chem. Phys. **40**, 939 (1964).
[61] J.-P. Hansen and I. McDonald, *Theory of Simple Liquids*, 2nd ed. (Elsevier, Amsterdam, 1986).
[62] A. Santos, S. Yuste, and M. de Haro, J. Chem. Phys. **117**, 5785 (2002).
[63] J. Barker and D. Henderson, Rev. Mod. Phys. **48**, 587 (1976).
[64] D. Henderson, Mol. Phys. **30**, 971 (1975).
[65] N. Carnahan and K. Starling, J. Chem. Phys. **51**, 635 (1969).
[66] B. Lubachevsky, *Proceedings of the International Workshop on Randomized Algorithms, Brno, Czech Republic*, edited by Rusins Freivalds, Lecture Notes Series (Electronic Colloquium on Computational Complexity, 1998), pp. 2610–2621.